J. Fluid Mech. (2008), *vol.* 599, *pp.* 121–168. © 2008 Cambridge University Press
doi:10.1017/S002211200700002X Printed in the United Kingdom

Dense granular flow down an inclined plane: from kinetic theory to granular dynamics

V. KUMARAN

Department of Chemical Engineering, Indian Institute of Science, Bangalore 560 012, India

(Received 16 February 2007 and in revised form 13 November 2007)

The hydrodynamics of the dense granular flow of rough inelastic particles down an inclined plane is analysed using constitutive relations derived from kinetic theory. The basic equations are the momentum and energy conservation equations, and the granular energy conservation equation contains a term which represents the dissipation of energy due to inelastic collisions. A fundamental length scale in the flow is the 'conduction length' $\delta = (d/(1-e_n)^{1/2})$, which is the length over which the rate of conduction of energy is comparable to the rate of dissipation. Here, d is the particle diameter and e_n is the normal coefficient of restitution. For a thick granular layer with height $h \gg \delta$, the flow in the bulk is analysed using an asymptotic analysis in the small parameter δ/h. In the leading approximation, the rate of conduction of energy is small compared to the rates of production and dissipation, and there is a balance between the rate of production due to mean shear and the rate of dissipation due to inelastic collisions. A direct consequence of this is that the volume fraction in the bulk is a constant in the leading approximation. The first correction due to the conduction of energy is determined using asymptotic analysis, and is found to be $O(\delta/h)^2$ smaller than the leading-order volume fraction. The numerical value of this correction is found to be negligible for systems of practical interest, resulting in a lack of variation of volume fraction with height in the bulk.

The flow in the 'conduction boundary layers' of thickness comparable to the conduction length at the bottom and top is analysed. Asymptotic analysis is used to simplify the governing equations to a second-order differential equation in the scaled cross-stream coordinate, and the resulting equation has the form of a diffusion equation. However, depending on the parameters in the constitutive model, it is found that the diffusion coefficient could be positive or negative. Domains in the parameter space where the diffusion coefficients are positive and negative are identified, and analytical solutions for the boundary layer equations, subject to appropriate boundary conditions, are obtained when the diffusion coefficient is positive. There is no boundary layer solution that matches the solution in the bulk for parameter regions where the diffusion coefficient is negative, indicating that a steady solution does not exist. An analytical result is derived showing that a boundary layer solution exists (diffusion coefficient is positive) if, and only if, the numerical values of the viscometric coefficients are such that volume fraction in the bulk decreases as the angle of inclination increases. If the numerical values of the viscometric coefficients are such that the volume fraction in the bulk increases as the angle of inclination increases, a boundary layer solution does not exist.

The results are extended to dense flows in thin layers using asymptotic analysis. Use is made of the fact that the pair distribution function is numerically large for dense flows, and the inverse of the pair distribution function is used as a small parameter. This approximation results in a nonlinear second-order differential equation for the pair distribution function, which is solved subject to boundary conditions. For a

https://doi.org/10.1017/S002211200700002X Published online by Cambridge University Press

dissipative base, it is found that a flowing solution exists only when the height is larger than a critical value, whereas the temperature decreases to zero and the flow stops when the height becomes smaller than this critical value. This is because the dissipation at the base becomes a larger fraction of the total dissipation as the height is decreased, and there is a minimum height below which the rate of production due to shear is not sufficient to compensate for the rate of dissipation at the base. The scaling of the minimum height with dissipation in the base, the bulk volume fraction and the parameters in the constitutive relations are determined. From this, the variation of the minimum height on the angle of inclination is obtained, and this is found to be in qualitative agreement with previous experiments and simulations.

1. Introduction

The flow of a granular material down an inclined plane has been studied extensively using computer simulations (Silbert *et al.* 2001, 2002; Mitarai & Nakanishi 2005) which incorporate sophisticated particle interactions for relatively large systems with heights of up to hundreds of particles. These provide detailed information about the density, mean velocity and granular temperature (mean-square fluctuating velocity) profiles. There are several remarkable features of the results of these simulations. The purpose of this analysis is to determine whether the salient features of these flows can be predicted by kinetic models, and the role of boundary interactions in determining the parameter ranges for which a steady solution can be obtained. There have been several studies of this flow, both phenomenological and kinetic-theory based (Louge & Keast 2001; Bocquet, Errami & Lubensky 2002; Ertas & Halsey 2002; Louge 2003; GDR MiDi 2004; Kumaran 2006*a*, *b*, *c*; Jenkins 2006) but a clear explanation for several of these features is still lacking.

Some of the salient features examined in the present study are listed below, along with attempts to provide a physical understanding of these features.

(*a*) The 'angle of repose' is defined as the angle at which the system transitions from a flowing to a static state as the angle of inclination is decreased. In most constitutive relations, a 'yield stress', which is independent of the rate of deformation, is used to obtain cessation of flow when the angle is decreased below the angle of repose. The total stress is defined as the sum of the yield stress, and a 'kinetic' stress which is dependent on the rate of deformation. A yield stress is expected at the initiation of flow when the material yields, and the value of the yield stress should be related to the relative arrangement of particles in the static state. Evidence from simulations (Silbert, Landry & Grest 2003) indicates that the angle of repose θ_{rep} is slightly lower than the maximum angle of stability θ_{max}, at which flow starts when the angle of inclination is increased. For $\theta > \theta_{max}$, the flow is continuous and the stress is described well by the Bagnold law. For $\theta_{rep} < \theta < \theta_{max}$, the velocity profile first deviates from the Bagnold profile, and then the flow becomes discontinuous avalanches when θ is very close to θ_{rep}. As the height of the layer is increased beyond 40 particle diameters, the difference $\theta_{max} - \theta_{rep}$ decreases to less than 1°, and the range of angles of inclination for which intermittent flow is observed is even smaller.

A 'yield' stress is not expected at the cessation of flow when the angle of inclination is decreased. When it stops, the stresses do not diverge; the shear and normal stresses are both linearly proportional to height, and they decrease continuously as the flow stops. Therefore, the resistance of the material to flow has to increase rapidly at a

https://doi.org/10.1017/S002211200700002X Published online by Cambridge University Press

finite angle of inclination, if the flow rate is to decrease sharply near cessation, and this rapid increase must be obtained using the same constitutive law that was used for the flowing state. This rapid increase has often been attributed to correlations of various kinds in the flow. It should be noted that the close packed nature of the system itself leads to correlations, since the movement of a particle at one point leads to the movement of particles a few diameters away. However, this correlation is already included in the theory via the divergence of the pair correlation function as the limit of close packing is approached. Apart from this, there have been many postulates of correlations decreasing over long distances (Ertas & Halsey 2002) or of clusters of particles (Bonamy *et al.* 2002) which transmit stresses over distances large compared to the particle diameter which could result in a yield stress even in the flowing state. Contact dynamics simulations (Lois, Carlson & Lemaitre 2005, 2006) do seem to show long chains of particles in contact extending over many particle diameters, but the same is not observed in discrete-element simulations, which show that the average coordination number (average number of particles in contact with a test particle) decreases much below 1 for inclined plane flows of materials such as sand and glass. Similarly, there have been experimental and simulation reports of correlations on the surface of granular flows (Pouliquen 2004; Baran *et al.* 2006). But there is no conclusive evidence for the presence of particle chains or eddies or coherent structures, which is surprising considering that simulations provide comprehensive information about these flows, at all length scales from the particle height to the layer width.

The initial postulates of correlations over long distances (Ertas & Halsey 2002) were motivated by the fact that there is a minimum height h_{stop} required for the material to flow, and the Froud number of a flow of thickness h has a stronger correlation with (h/h_{stop}) than with the height scaled by the particle diameter. It was postulated that h_{stop} is a measure of the length of the correlations in the flowing state, and this length diverges as the minimum angle for flow of an infinite layer is approached. However, the idea of diverging correlation lengths is in contradiction with the assumption of local rheology. The rheological model will be valid only if the thickness of the differential volume considered is larger than the correlation length; if it is smaller than the correlation length, its surface would break though a chain of particles or an eddy, and the stress response would depend on the dimensions of the volume considered. When the correlation length diverges it should be comparable to the system size at some point, and at this point the assumption of local rheology is invalid. There have been studies (Jop, Forterre & Pouliquen 2006) which indicate that the rheology is local, in which case there cannot be long-range correlations over many particle diameters in these flows.

It was shown in an earlier study (Kumaran 2006*a*) that constitutive relations derived from kinetic theory could predict both the cessation of flow at a finite angle and the decrease in volume fraction with an increase in the angle of inclination, provided the microscopic model was sufficiently realistic, and terms up to Burnett order were retained in the constitutive relation. That study employed analytical calculations of the viscometric coefficients up to Burnett order, and both numerical and asymptotic evaluation of these coefficients for two different particle models. However, that study was restricted to the prediction of volume fractions in the bulk of the flow where the volume fraction is nearly a constant. A subsequent study (Jenkins 2006) used a modification of the dissipation term in the energy balance equation in order to obtain the same qualitative features, and used numerical solutions of the governing equations to obtain the density and temperature profiles. Here, we use asymptotic

https://doi.org/10.1017/S002211200700002X Published online by Cambridge University Press

analysis to examine how the results are altered due to the presence of the boundaries at the top and bottom.

(*b*) The volume fraction of the particles is a constant in the bulk of the flow, the granular temperature and all stress components are linear functions of height, and the mean strain rate increases as the square root of the height from the bottom of the layer. The volume fraction is found to be, within numerical accuracy, independent of position in the flow (apart from thin layers at the top and bottom of thickness about 3–5 particle diameters where the volume fraction varies with position), independent of the total height of the material, and dependent only on the angle of inclination of the inclined plane. In addition, the volume fraction does not seem to depend on the boundary conditions at the top and bottom surfaces, and the effects of the boundaries seem to affect the flow only within layers of width 3–5 particle diameters at the boundaries. In the earlier study (Kumaran 2006*a*), a small parameter was identified, which was the ratio of the 'conduction length' (to be discussed later) and the height of the flowing layer. It was shown that when this parameter is small, there is a balance between the source of energy due to shear and the dissipation due to inelastic collisions in the bulk. A direct consequence of this is that the volume fraction is a constant in the bulk. To make quantitative predictions of the dependence of the volume fraction on angle of inclination, the asymptotic analysis was carried out in the close packing limit using the inverse of the pair distribution function as a small parameter. In a subsequent study (Kumaran 2006*b*), the correction to the volume fraction due to the conduction of energy was analysed using an expansion in the ratio of the conduction length and layer height, and it was concluded that the correction is very small for the parameters used in the simulations. The study of Jenkins (2006) numerically predicted nearly constant density profiles in the bulk, with a modification of the energy dissipation term due to long-range correlations. Here, we compare the asymptotic solution for the correction to the density in the bulk with the complete numerical solution of the momentum and energy equations.

(*c*) There are regions at the top and bottom where the volume fraction varies from the constant value in the bulk. In the present analysis, we identify these regions as 'conduction boundary layers' at the top and bottom where the rate of conduction of energy is comparable to the rates of production and dissipation. An asymptotic analysis in the ratio of the conduction length and the layer height is used to reduce the differential equation to a diffusion equation in the bottom layer, and analytical solutions for the boundary layer profiles are obtained. A slightly more complicated ordinary differential equation is obtained, and solved, for the top layer.

(*d*) Simulations (Silbert *et al.* 2001) also report that a steady flow is possible only over a very limited range of parameters in the particle interaction model. For a linear contact model, solutions are found only when the coefficient of restitution is less than about 0.92, and in the presence of frictional interactions between the particles. In the present study, we identify one of the limitations to the existence of solutions, which is the existence of boundary layer solutions. In the simplified boundary layer equations, solutions which decay into the bulk exist only when the diffusion coefficient is positive. When the diffusion coefficient is negative, there are no boundary layer solutions possible.

(*e*) An often-cited feature of the flow down an inclined plane is the h_{stop} vs. angle of inclination curve (Pouliquen 1999; Silbert *et al.* 2001). In experiments, after a granular layer has flowed down an incline, there is a residual layer of thickness h_{stop} remaining on the inclined plane, and the thickness of this layer decreases as the angle of inclination increases. The residual layer has been linked, previously, to the presence

https://doi.org/10.1017/S002211200700002X Published online by Cambridge University Press

of correlations in the flow (Ertas & Halsey 2002), and the thickness of this layer has been related to the correlation length.

In the present analysis, we relate the thickness of the static layer to the dissipation in the base. In a thin flowing layer, there is a balance between the rate of shear production and the rate of dissipation due to inelastic inter-particle collisions and particle–base collisions. As the layer thickness becomes smaller, the fraction of the dissipation due to particle–base collisions becomes larger, and there is a minimum layer thickness below which the rate of shear production is insufficient to balance the rate of dissipation, resulting in the collapse of the flowing layer. In order to analyse this phenomenon for thin layers, we first reduce the governing equations to a second-order nonlinear equation using an asymptotic expansion. The largeness of the pair distribution function in dense flows is used to advantage in the analysis, and the small parameter is the inverse of the pair distribution function.

The phenomenological 'mixing length' theories (Ertas & Halsey 2002; GDR MiDi 2004) attempt to obtain the ratio of the shear and normal stress as a function of the strain rate scaled by the normal stress. In this sense, this is different from classical rheology, which is an attempt to determine the different components of the stress as a function of the strain rate. These studies do find universal relations for a given flow type in the dense inertial regime for a layer of thickness 15 particle diameters or larger. These studies also define a 'coherence length' or a 'correlation length' as $(\tau/(\rho\dot{\gamma}^2))^{1/2}$, where τ is the shear stress, ρ is the mass density and $\dot{\gamma}$ is the strain rate. It is found that the correlation length could be large, as much as 20–40 particle diameters. This is unexpected, because if there are correlations, one would not expect the rheology to be the same for length scales less than the correlation length. The contradiction arises from the fact that in dense collisional flows, momentum transport takes place due to collisions, and the collision frequency diverges proportionally to the pair correlation function as the random close packed limit is approached. The divergence of the pair correlation function should also be incorporated into the definition of the correlation length. If a correlation length is defined as $(\tau/(\rho\chi\dot{\gamma}^2))^{1/2}$, where χ is the pair correlation function, the correlation length will not be large compared to a particle diameter, and the rheology would be expected to be local. In addition, these studies also find that there is a difference in the rheology between the bulk and the surface layers. In the present analysis, the characteristic length scale that accounts for this difference is the conduction length. In the bulk where the distance from a boundary is large compared to the conduction length, there is a balance between the rates of production and dissipation of energy, and the stresses are proportional to the square of the strain rate, from dimensional analysis. In boundary layers of thickness comparable to the conduction length, energy conduction is important, and the constitutive relation will depend on the strain rate as well as the perturbation to the temperature caused by the boundaries.

There have been several studies which have used constitutive relations derived from kinetic theory. In some studies, numerical solutions of the governing equations are used to predict volume fraction and temperature profiles, with a set of boundary conditions for the temperature and flux at the top and bottom surfaces. Some of these studies (Bocquet *et al.* 2002; Jenkins 2006) have used viscometric coefficients obtained from kinetic theories for inelastic particles. The objective of these studies was to obtain profiles that appear similar to those in simulations, particularly the constant volume fraction in the bulk. While Bocquet *et al.* (2002) modified the coefficient of viscosity based on theories for the glass transition, Jenkins (2006) modifed the energy dissipation term by postulating a correlation length in order to obtain profiles that

https://doi.org/10.1017/S002211200700002X Published online by Cambridge University Press

look qualitatively similar to those observed in experiments. These numerical solutions of the momentum and energy equations, in which the constitutive relations are derived from kinetic theory, have played a very important role in advancing the understanding of the physics of granular flows. However, they have to be analysed with caution when the underlying equations are nonlinear. The absence of convergence to a final solution from some initial guess does not imply that no solution exists. Conversely, the numerical convergence to a solution to within a certain accuracy does not imply that the solution is real, or that the same solution will be obtained when the accuracy required is made more stringent. Nonlinear problems also have the difficulty that there are multiple solutions. A difficulty specific to dense granular flows is that the constitutive relations contain a pair distribution function, which diverges rapidly as the limit of close packing is approached. Small variations in the volume fraction lead to large variations in the pair distribution function, thus making numerical convergence difficult.

There have been studies (Jenkins & Askari 1999; Louge & Keast 2001; Louge 2003) which have attempted to separate the flow into a bulk flow and boundary layers, and then solve for these separately. The balance equations in the different regions are different, and different criteria are used to patch the solutions at pre-defined locations. While the separation into different regions is carried out on the basis of some physical approximations motivated by observations, these solutions cannot be strictly classified as matched asymptotic expansions. In matched asymptotic expansions, the governing equations are the same in different regions, but are approximated in different ways to obtain the solutions in the different regions. These approximate solutions are then matched to obtain a composite solution. Another drawback of the aforementioned boundary layer theories is that the equation for the fluctuating velocity (square root of temperature) in the boundary layers is a linear equation. For these types of solutions, a matching procedure cannot be used because the solution either decreases to zero or diverges when there is a transition from the boundary layer to the bulk. This problem is overcome by Louge (2003) and Jenkins & Askari (1999) by patching solutions at specified locations in the domain. The disadvantage of this procedure is that it results in the solution being dependent on where the patching is done, and which function or its derivatives are patched. In the physical system, there is no specified location for the transition from the boundary layer to the bulk flow; rather, the solutions in the two regions should match in the intermediate region where, simultaneously, the inner coordinate goes to infinity and the outer coordinate goes to zero. Here, we show that the boundary layer equation for the square root of the temperature is a nonlinear equation, and this permits us to obtain a matched asymptotic solution.

The goal of the present analysis is to specify a simple set of equations which is valid throughout the flow, and then to use asymptotic techniques to simplify the equations in the bulk and in the boundary layers. We use the analytical solutions, as well as numerical solutions of the simplified equations, to obtain a better understanding of the qualitative features of the flow down an inclined plane. Though the viscometric coefficients for the rough particle model are used for quantitative estimates of the field variables, the emphasis is on the forms of the equations obtained as a function of parameters that can be evaluated for any particle model. It should be emphasized that the numerical results obtained here will not be comparable to those in experiments and simulations, just as the stress obtained from one model fluid cannot be quantitatively compared with experiments on another fluid with different viscosity. However, if the form of the constitutive equations is correct, then the functional forms of the

https://doi.org/10.1017/S002211200700002X Published online by Cambridge University Press

dynamical variables obtained from the theory will be in agreement with those observed in simulations and experiments.

One of the motivations for using matched asymptotic analysis is the observation in simulations that the temperature boundary condition at the bottom affects the dynamical fields only in a thin layer at the bottom, but not in the bulk. This is similar to the situation that existed at the beginning of the last century (Anderson 2005), with respect to the effect of solid surfaces on the velocity fields in high-Reynolds-number flows of Newtonian fluids. It was first shown by Prandtl (Anderson 2005) that the effects of boundaries are confined to thin regions near the surface where viscous effects are important, unless there is boundary layer separation in the flow past bluff bodies. This study also used, for the first time, the technique of matched asymptotic expansions to match the boundary layer and outer flow solutions. Here, we suggest that a similar situation occurs for the temperature field in a granular flow, because energy is not a conserved variable. The asymptotic analysis provides some insight which would otherwise be difficult to obtain from numerical solutions. For example, it is shown analytically that a boundary layer solution exists only for some values of the viscometric coefficients, and it exists only if the volume fraction decreases as the angle of inclination increases in the bulk. Such a definitive result would not be obtained by carrying out computations over large swathes of parameter space.

One of the important results of simulations (Silbert *et al.* 2001) is that the granular flow down an inclined plane satisfies the Bagnold law, which states that the stress is proportional to the square of the strain rate. This observation is significant. The Bagnold law is a dimensional necessity if the only relevant time scale is the inverse of the strain rate, and the dynamics is not affected by any material time scales, such as the period of the inter-particle interactions. Note that the duration of an inter-particle interaction cannot significantly exceed the strain rate, because the particles are convected past each other over a time period comparable to the inverse of the strain rate. The constitutive relation for the stress assumes different forms in different regimes, depending on the parameter $\dot{\gamma}\tau_c$, which is the ratio of the time of contact τ_c and the flow time, which is the inverse of the strain rate $\dot{\gamma}$. In the quasi-static regime, $\dot{\gamma}\tau_c \sim 1$, the stresses are found to be independent of the strain rate, because the transmission of stress is due to contact forces between particles. For a dilute granular flow, interactions can be modelled as instantaneous collisions for $\dot{\gamma}\tau_c \ll 1$. However, for dense flows, the collision frequency increases proportionally to the pair distribution function at contact χ, and the period of an interaction is small compared to the time between interactions for $\dot{\gamma}\tau_c\chi \ll 1$. In this limit, the stress is not dependent on the period of a collision, and from dimensional analysis it can be inferred that the stress is proportional to the square of the strain rate (Bagnold law). As the strain rate is increased from the quasi-static regime, there is a gradual transition from the frictional rate-independent stress law to the Bagnold law. Simulations using the discrete element method (DEM) (Silbert *et al.* 2001), where the particle interactions are modelled using a spring–dashpot model, indicate that the Bagnold law is valid even when the average number of contacts per particle is larger than 1, and Bagnold coefficients do not change very much as τ_c is reduced and the system transitions to a binary contact regime. More recent DEM simulations of Reddy and Kumaran (2007) have shown that the average coordination number in a dense flow decreases rapidly with an increase in the spring constant of the particles, and the average coordination number is smaller than 1 for spring constants appropriate for real materials such as sand and glass beads (the simulations of Silbert *et al.* 2001 were performed with

https://doi.org/10.1017/S002211200700002X Published online by Cambridge University Press

spring constant about four orders of magnitude smaller than for sand or glass spheres in order to reduce computational time). In addition, even though there are multiple contacts at low spring constants, the force on the particle is dominated by the force in one contact, which is larger in magnitude than the forces in all other contacts. Silbert *et al.* (2007) studied the contact lifetime distributions of dense granular flows using the DEM, and found that the dominant mode of interaction is brief binary collisions, rather than a large number of long-lived contacts. This indicates that the binary collision approximation is, in fact, a good approximation for dense granular flows. It should, however, be noted that the Bagnold law is valid only in the bulk, where there is a balance between the rates of production and dissipation of energy. Conduction of energy is significant in boundary layers of thickness comparable to the conduction length at the boundaries, where the Bagnold law is not valid.

Kinetic theories for granular materials exploit the analogy between the motion of discrete particles in the granular material and the motion of molecules in a molecular gas. There have been many derivations of constitutive relations for granular materials. These include approximate approaches that modified the Navier–Stokes equations by adding a dissipation term due to inelastic collisions in the energy equation (Savage & Jeffrey 1981; Jenkins & Savage 1983; Lun *et al.* 1984; Jenkins & Richman 1985; Kumaran 1998), as well as asymptotic approaches that used expansions in the inelasticity and the Knudsen number (Sela, Goldhirsch & Noskowicz 1996; Sela & Goldhirsch 1998; Kumaran 2004, 2006*a*). The important difference between a molecular gas and the granular flow of inelastic particles is that energy is not a conserved variable in a granular flow, since energy is dissipated in inter-particle collisions. The details of the constitutive relations used here are provided in the next section.

It is usually assumed that these theories are applicable only in the dilute limit, where the mean free path is large compared to the particle diameter, and the assumptions of molecular chaos are valid. However, as noted earlier, the simulations (Silbert *et al.* 2001) have shown that the Bagnold law for the stress tensor, which is a consequence of the kinetic theory calculation, applies even for dense granular flows with volume fraction ranging from 0.55 to about 0.58. In addition, it is known (Mitarai & Nakanishi 2005; Kumaran 2006*a*, *b*) that many of the features of the flow can be predicted using kinetic theory. If the rate of conduction of energy is neglected in the energy balance equation, kinetic theory predicts that the density is independent of height in the bulk of the flow. One of the drawbacks of constitutive relations derived earlier for granular flows (Savage & Jeffrey 1981; Jenkins & Richman 1985) was that these predicted that the density in the flow increases as the angle of inclination is increased, which is unphysical, because one would expect the density to decrease and the layer to swell as the angle of inclination is increased. A recent theory (Jenkins 2006) attempted to overcome this problem by postulating the presence of a 'correlation length' for the energy dissipation rate. This was motivated by the study Mitarai & Nakanishi (2005) which showed that the dissipation rate in two-dimensional simulations is lower than the kinetic theory predictions, and also based on similar results from contact dynamics studies (Lois *et al.* 2005, 2006).

The kinetic theory approach for gases is valid only in the dilute limit, owing to the molecular chaos approximation that is made while calculating the collision integral. For dense gases, the Enskog approximation is used, where the two-particle velocity distribution function is written as the product of the single-particle velocity distribution function and the equilibrium pair correlation function. It is known that

https://doi.org/10.1017/S002211200700002X Published online by Cambridge University Press

the molecular chaos approximation breaks down in molecular fluids owing to the presence of correlations in the velocities of colliding particles. In order to incorporate collisions, it is necessary to solve the 'ring kinetic equation', where the three-particle distribution function is expressed in terms of the two-particle distribution functions. The effect of correlations has been calculated for molecular gases (Ernst *et al.* 1978), and it has been shown that the inclusion of correlations at the three-particle level leads to a divergence in the viscosity in two dimensions, and a divergence in the Burnett coefficient in three dimensions. If the shear stress is expanded as a function of the strain rate $\dot{\gamma}$ for a linear shear flow, the leading (Navier–Stokes) term is proportional to $\dot{\gamma}$, while the next higher 'Burnett' term is proportional to $\dot{\gamma}^2$. When the number density increases, there is a contribution to the stress due to correlations in the particle positions prior to collision (Ernst *et al.* 1978) which are incorporated in the 'ring kinetic equation'. The leading correction to the stress due to correlated collisions is proportional to $|\dot{\gamma}|^{3/2}$, which is non-analytic in the limit of zero strain rate, resulting in the divergence of the Burnett coefficients.

It turns out that correlations do not cause divergence in the transport coefficients for granular flows (Kumaran 2006*c*), because the natures of the hydrodynamic modes in granular flows are very different. In molecular fluids, there are five conserved (slow) modes: the mass, three components of the momentum and energy. Of these, there are three transverse modes (energy and two transverse components of the momentum) which are diffusive, and have a real decay rate proportional to k^2 in the limit $k \to 0$, where k is the wavenumber. The other two longitudinal modes (density and longitudinal momentum) are propagating, for which the decay rate has an imaginary component proportional to k and a real component proportional to k^2. It turns out that the hydrodynamic modes for a sheared granular flow are very different, because energy is not a conserved variable, and there are only four slow modes. It has been shown (Kumaran 2004) that the decay rates of these modes are proportional to $k^{2/3}$ in the limit $k \to 0$. Using these hydrodynamic modes, a ring kinetic calculation (Kumaran 2006*c*) for a granular fluid has shown that there are no divergences in the viscosity and Burnett coefficients for a sheared granular flow in three dimensions. Thus, the regular Enskog expansion is valid for a dense granular flow, provided the distortion of the pair correlation function due to the flow is taken into account.

In the present analysis, we determine the effect of conduction on the density profile in the bulk of a steady granular flow down an inclined plane, as well as in the boundary layers. In the bulk, we use asymptotic analysis to determine the corrections to the density and temperature profiles due to the conduction term in the energy equation, and show that the corrections are small. This provides an explanation for the remarkable lack of variation of density observed in simulations. In the boundary layers at the top and bottom, where the conduction term in the energy balance equation is comparable to the source and dissipation terms, we determine the conditions under which boundary layer solutions exist. Further, we proceed to obtain analytical expressions for the temperature field in the limit where the pair correlation function is large compared to 1, using an expansion in the inverse of the pair distribution function. Asymptotic matching is then used to obtain a solution which is valid both in the bulk and in the two boundary layers. Finally, a nonlinear equation is derived for the temperature, which is valid when the pair distribution function is large compared to 1. The solution of this equation for thin layers is examined, in order to determine the dependence of the minimum height required for flow on the angle of inclination.

https://doi.org/10.1017/S002211200700002X Published online by Cambridge University Press

2. Constitutive relations

The analysis is carried out for two of the three particle models that were previously studied (Kumaran 2006*a*). In the case of 'smooth nearly elastic particles' the relative velocity of the particles along the line joining their centres after collision is $-e_n$ times the relative velocity before collision, while the relative velocity perpendicular to the line joining the centres is unchanged in the collision. The analysis of Kumaran (2006*a*) showed that realistic results, such as the decrease in the volume fraction with an increase in the angle of inclination, are not obtained for the smooth nearly elastic particle model, and so we do not use this model. Here, quantitative comparisons are made for the 'rough nearly elastic' particle model and the 'partially rough nearly elastic' particle model. In the case of rough nearly elastic particles, the particle rotation is also incorporated in the description, and the relative velocity of the particles in the direction of the line joining their centres is $-e_n$ times the relative velocity before collision, while the relative velocity perpendicular to the line joining their centres after collision is $-e_t$ times the relative velocity before collision. The normal coefficient of restitution e_n varies between 0 and 1; $e_n = 1$ corresponds to perfectly elastic collisions, while $e_n = 0$ corresponds to perfectly inelastic collisions. The tangential coefficient of restitution e_t varies between -1 and $+1$: $e_t = -1$ corresponds to smooth particles where there is no change in the relative velocity after collision, while $e_t = 1$ corresponds to perfectly rough particles where the relative velocity perpendicular to the line joining their centres is reversed after the collision. Energy is conserved for both $e_t = +1$ and $e_t = -1$, and it is convenient to carry out an asymptotic analysis about the limit where energy is conserved. In the case of the partially rough particle model, collisions are considered to be smooth if the angle between the relative velocity vector and the line joining their centres is greater than a 'roughness angle' θ_r, and considered to be rough otherwise.

The basic equation used is the inelastic Enskog equation, and the details of the derivation are discussed in Kumaran (2004, 2006*a*). The velocity distribution function is assumed to be an anisotropic Gaussian in both the linear and angular velocities. An expansion is carried out about the elastic limit in the parameter $\varepsilon = (1 - e_n)^{1/2}$, where e_n is the coefficient of restitution. In the case of rough particles, the ratio $(1 - e_t)/(1 - e_n)$ is considered to be $O(1)$ in the expansion. The leading-order, $O(\varepsilon)$ and $O(\varepsilon^2)$, equations are solved to obtain the corresponding distribution functions. The constitutive relations are then determined from the solutions for the distribution function. The viscometric coefficients obtained in this manner are approximate due to the assumption that the solution is an anisotropic Gaussian. This approximation is equivalent to retaining the first term in the Sonine polynomial expansion for the first and second corrections to the distribution function. For an elastic gas, the correction to the viscosity due to the neglect of the next higher term is 1.2 %, and the correction to the Burnett coefficients is about 6 %.

We use a uniform approximation for the constitutive relation which is valid in the limits where the length scale is large and small compared to the conduction length. We discuss the constitutive relations appropriate for both these limits first, and then the uniform approximation is provided. The mass of a particle is set equal to 1 in the present calculation, so that all parameters are non-dimensionalized by particle mass, and the temperature has units of the square of velocity. The conduction length is determined by a balance between the rates of thermal diffusion and dissipation. The divergence of the heat flux is $\rho D_T (T/L^2)$, where T is the temperature, L is the length scale over which the temperature varies. The thermal diffusivity $D_T \sim \lambda T^{1/2}$, where λ is the microscopic scale (mean free path in a dilute gas and particle diameter in a

https://doi.org/10.1017/S002211200700002X Published online by Cambridge University Press

dense gas). The rate of dissipation is proportional to $(\rho\varepsilon^2 T^{3/2}/\lambda)$, since dissipation of energy in a collision is proportional to $(1-e_n)T$, and the collision frequency is proportional to $(T^{1/2}/\lambda)$. A balance between the rates of conduction and dissipation is obtained only for $L = L_c \sim (\lambda/\varepsilon)$, where L_c is the conduction length.

If the macroscopic scale, which is the height of the flowing layer h in the present system, is large compared to the conduction length, the rate of conduction of energy is small compared to the rate of dissipation. The temperature is determined by a local balance between the rates of production and dissipation, and the energy balance reduces to

$$2\mu S_{ij} S_{ji} - D = 0 \tag{2.1}$$

where μ is the viscosity, S_{ij} is the symmetric part of the rate of deformation tensor G_{ij}, and D is the rate of dissipation of energy. The stress is expressed in terms of the symmetric part S_{ij}, the antisymmetric part A_{ij} and the isotropic part of the rate of deformation tensor G_{ii}, as well as in terms of the temperature gradients. The most general expression for the stress obtained using the leading-order first and second corrections to the distribution function is (Chapman & Cowling 1970)

$$\begin{aligned}
\sigma_{ij} = & -p(\phi, S_{ij}, G_{ii})\delta_{ij} + 2\mu(\phi, S_{ij} G_{ii}) S_{ij} + \mu_b(\phi, S_{ij}, G_{ii})\delta_{ij} G_{kk} \\
& + \mathscr{A}_{SS} S_{ik} S_{kj} + \mathscr{A}_{SG} S_{ij} G_{kk} + \mathscr{A}_{SAS}(S_{ik} A_{kj} + S_{jk} A_{ki}) \\
& + \mathscr{A}_{AA} A_{ik} A_{kj} + \mathscr{A}_{SAA}(A_{ik} S_{kj} - S_{ik} A_{kj}) \\
& + \mathscr{C}_S \left(\frac{\partial}{\partial x_i}\left(\frac{1}{\rho}\frac{\partial p}{\partial x_j}\right) + \frac{\partial}{\partial x_j}\left(\frac{1}{\rho}\frac{\partial p}{\partial x_i}\right) - \frac{2\delta_{ij}}{3}\frac{\partial}{\partial x_k}\left(\frac{1}{\rho}\frac{\partial p}{\partial x_k}\right)\right) \\
& + \frac{\delta_{ij}}{3}\left(\mathscr{B}_{SS} S_{kl} S_{lk} + \mathscr{B}_{AA} A_{kl} A_{lk} + \mathscr{B}_{GG} G_{kk}^2 + \mathscr{C}_I \frac{\partial}{\partial x_k}\left(\frac{1}{\rho}\frac{\partial \sigma_{kl}}{\partial x_l}\right)\right) \\
& + \mathscr{C}_A \left(\frac{\partial}{\partial x_j}\left(\frac{1}{\rho}\frac{\partial p}{\partial x_i}\right) - \frac{\partial}{\partial x_i}\left(\frac{1}{\rho}\frac{\partial p}{\partial x_j}\right)\right) \\
& + \mathscr{D}\left(\frac{\partial}{\partial x_i}\frac{\partial}{\partial x_j} - \frac{\delta_{ij}}{3}\frac{\partial^2}{\partial x_k^2}\right) T \\
& + \frac{\mathscr{E}}{T}\left(\frac{\partial T}{\partial x_i}\frac{\partial T}{\partial x_j} - \frac{\delta_{ij}}{3}\frac{\partial T}{\partial x_k}\frac{\partial T}{\partial x_k}\right) \\
& + \frac{\mathscr{F}}{\rho T}\left(\frac{1}{2}\frac{\partial p}{\partial x_i}\frac{\partial T}{\partial x_j} + \frac{1}{2}\frac{\partial T}{\partial x_i}\frac{\partial p}{\partial x_j} - \frac{\delta_{ij}}{3}\frac{\partial T}{\partial x_k}\frac{\partial p}{\partial x_k}\right).
\end{aligned} \tag{2.2}$$

Note that the mass of the particle has been set equal to 1 without loss of generality, and from dimensional analysis, all the Burnett coefficients above have dimensions of inverse length. In (2.2) we retain the pressure and the viscous terms, and the Burnett terms proportional to $\mathscr{A}$ and $\mathscr{B}$, and neglect all other terms, for the following reason. The Burnett terms proportional to $\mathscr{A}$ and $\mathscr{B}$ are proportional to the square of the strain rate, $\dot{\gamma}^2$. The terms proportional to $\mathscr{C}$ to $\mathscr{F}$ are all proportional to (T/h^2), where h is the macroscopic scale. The temperature and strain rate can be compared by examining the energy balance equation (2.1), in which the viscosity is proportional to $(T^{1/2}/d^2)$, and the rate of dissipation of energy per unit volume is proportional to $(\rho\varepsilon^2 T^{3/2}/\lambda)$. For a dense flow, $\rho \sim (1/d^3)$, and $\lambda \sim d$, so the temperature scales as $T \sim (\dot{\gamma} d/\varepsilon)^2 \sim (L_c\dot{\gamma})^2$. This can be used to compare the terms proportional to the square of the strain rate and the temperature gradient in (2.2). The terms proportional to the strain rate scale as $\dot{\gamma}^2$, while those proportional to the second spatial derivative of the temperature and pressure scale as $(\dot{\gamma} L_c/h)^2$, where h, the height of the flowing

https://doi.org/10.1017/S002211200700002X Published online by Cambridge University Press

layer, is the macroscopic length scale in the present problem. For $(L_c/h) \ll 1$, the terms proportional to the second derivative of the temperature can be neglected compared to the terms proportional to the square of the strain rate. Therefore, we retain the terms proportional to $\mathscr{A}$ and $\mathscr{B}$ in (2.2), and neglect all other terms.

The reasons the terms proportional to $\mathscr{A}$ and $\mathscr{B}$ are retained here are twofold. First, it has been shown (Kumaran 2004) that the decay rate of the hydrodynamic modes in a uniformly sheared granular flow depends on the coefficients $\mathscr{A}$ and $\mathscr{B}$ in the long wave limit. In the present system, the terms proportional to $\mathscr{A}$ and $\mathscr{B}$ are necessary to capture the normal stress differences. It has been observed in simulations (Silbert *et al.* 2001) that the first normal stress is close to zero in these flows, but the second normal stress is significant. We examine whether the predictions are in agreement with the observations by retaining the normal stress terms. It should be noted that the constitutive relation (2.2) was derived assuming a balance between the rates of production and dissipation of energy (equation (2.1)), and so the constitutive relation for the heat flux cannot be derived in a similar manner.

In the limit where the conduction length is comparable to the macroscopic length scale, $L_c \sim L$, the rate of dissipation is small compared to the rate of conduction. The energy balance equation is of the form

$$\frac{\partial}{\partial x_i}\left(K\frac{\partial T}{\partial x_i}\right) + 2\mu S_{ik}S_{ki} - D = 0. \tag{2.3}$$

The constitutive relation for the heat flux was derived using the usual expansion in the gradients of the temperature (Chapman & Cowling 1970). Here, we have retained the term proportional to the temperature gradient in the equation for the heat flux. For inelastic fluids, there is an additional term proportional to the density gradient in the equation for the heat flux (Sela & Goldhirsch 1998). The contribution of this term to the heat flux turns out to be small in the present case, because the density is nearly a constant in a dense flow, and so it is not included here. In the constitutive relation for the stress, the temperature still scales as $(\dot{\gamma}L_c)^2$, but the length scale for the gradients is L_c instead of the macroscopic length h. In this case, it can easily be seen that the pressure $p \sim \rho T \sim ((\dot{\gamma}L_c)^2/d^3)$, $\mu S_{ij} \sim (\dot{\gamma}^2 L_c/d^2)$, while all the Burnett terms are proportional to $(\dot{\gamma}^2/d)$. Therefore, each successive term in the expansion is factor (d/L_c) smaller than the previous term, and we use the usual expression for the stress tensor which includes just the pressure and viscous terms:

$$\sigma_{ij} = -p\delta_{ij} + 2\mu S_{ij} + \mu_b \delta_{ij} G_{kk}. \tag{2.4}$$

It should be noted that the divergence of the heat flux in the energy equation is small in comparison to the rates of production and dissipation in the bulk of the flow, where the Burnett terms in the equations for the stress are included in order to capture the normal stress differences. Therefore, it is not necessary to include the Burnett terms for the heat flux in this region. The divergence of the heat flux is included in the boundary layers at the top and bottom, but the expansion in these regions is truncated at the Navier–Stokes order, for reasons mentioned above (2.4). As a uniform approximation valid in both regimes, (2.3) is used for the heat conduction equation, even though the rate of conduction is small compared to the rates of production and dissipation in the bulk of the flow for $h \gg L$. In the equation for the stress (2.4), the pressure and viscous terms, as well as the terms proportional to $\mathscr{A}$ and $\mathscr{B}$ are included, but the contribution due to these terms is small in the

https://doi.org/10.1017/S002211200700002X Published online by Cambridge University Press

	Rough	Partially rough
p_ϕ	$(6\phi/\pi)(1+2(2-\varepsilon^2)\phi\chi)$	$(6\phi/\pi)(1+2(2-\varepsilon^2)\phi\chi)$
μ_ϕ	$(0.195/\chi)+0.892\phi+3.112\phi^2\chi$	$(0.196/\chi)+0.713\phi+2.464\phi^2\chi$
D_ϕ	$(144/\pi^{3/2})\phi^2\chi(1+a_t)$	$(144/\pi^{3/2})\phi^2\chi(1+a_t/4)$
K_ϕ	$(1.014/\chi)+5.015\phi+19.27\phi^2\chi$	$(0.719/\chi)+3.781\phi+12.426\phi^2\chi$
B_ϕ	$(0.04094/\chi)+(0.00433/\phi\chi^2)$	$(0.09601/\chi)+(0.00292/\chi^2\phi)$
	$-0.191\phi-1.05\phi^2\chi$	$-0.01752\phi-1.43367\phi^2\chi$

TABLE 1. Viscometric coefficients obtained from kinetic theory for rough and partially rough nearly elastic spheres in three dimensions (Kumaran 2006*a*). Here, $a_t=(1-e_t)/(1-e_n)$. In the above relations, particle mass is set equal to 1.

conduction boundary layers. The expression used for the stress is

$$\begin{aligned}\sigma_{ij} = &-p(\phi, S_{ij}, G_{ii})\delta_{ij} + 2\mu(\phi, S_{ij}G_{ii})S_{ij} + \mu_b(\phi, S_{ij}, G_{ii})\delta_{ij}G_{kk}\\ &+ \mathscr{A}_{SS}S_{ik}S_{kj} + \mathscr{A}_{SG}S_{ij}G_{kk} + \mathscr{A}_{SAS}(S_{ik}A_{kj}+S_{jk}A_{ki})\\ &+ \mathscr{A}_{AA}A_{ik}A_{kj} + \mathscr{A}_{SAA}(A_{ik}S_{kj}-S_{ik}A_{kj})\\ &+ \tfrac{1}{3}\delta_{ij}\left(\mathscr{B}_{SS}S_{kl}S_{lk} + \mathscr{B}_{AA}A_{kl}A_{lk} + \mathscr{B}_{GG}G_{kk}^2\right).\end{aligned} \tag{2.5}$$

The pressure, viscosity and the coefficients $\mathscr{A}$ and $\mathscr{B}$ are found from an earlier calculation (Kumaran 2006*a*). Not all of these coefficients are required for the present calculation, since we are considering a uni-directional flow in which the isotropic part of the rate of deformation tensor is zero. The coefficients used in the present analysis are summarized in table 1.

The pair distribution function used here is of two types, the Carnahan–Starling pair distribution function,

$$\chi(\phi) = (2-\phi)/(2(1-\phi)^3), \tag{2.6}$$

and the high-density pair distribution function due to Torquato (1995),

$$\chi(\phi) = \frac{(2-\phi_f)}{2(1-\phi_f)^3}\frac{\phi_c-\phi_f}{\phi_c-\phi}, \tag{2.7}$$

where $\phi_c=0.64$ and $\phi_f=0.49$. The Carnahan–Starling pair distribution function is accurate at low and moderate densities, but does not show the expected divergence as the random close packing limit is approached. The high-density pair distribution is not accurate at low densities, but shows the expected divergence proportional to $(\phi_c-\phi)^{-1}$ as the close packing limit is approached, where ϕ is the volume fraction and ϕ_c is the volume fraction at random close packing. Though the Carnahan–Starling pair distribution function does not diverge at close packing and diverges only at the unphysical value of $\phi=1$, we present some results for this pair distribution to show that the velocity and temperature profiles are not sensitive to the nature of the pair distribution function, so long as the pair distribution function is numerically large for the flow under consideration.

3. Bulk flow

The granular material is composed of hard-sphere particles of diameter d flowing down a plane inclined at an angle θ to the horizontal. A Cartesian coordinate

https://doi.org/10.1017/S002211200700002X Published online by Cambridge University Press

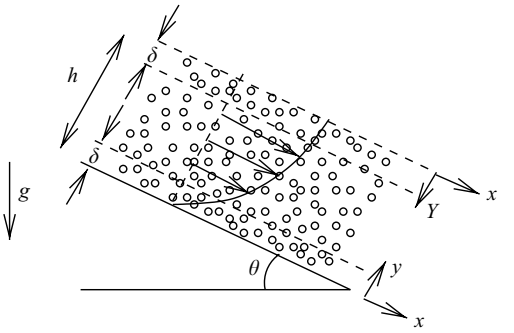


FIGURE 1. Configuration and coordinate system.

system is used, where the velocity and velocity gradient are in the x- and y-directions respectively, as shown in figure 1. It should be noted that throughout the analysis, the mass of a particle is set equal to 1 for simplicity, so that the mass dimension is scaled by the particle mass. The shear and normal stress balances are

$$(\mathrm{d}\sigma_{xy}/\mathrm{d}y) = -\rho g \sin(\theta), \quad (\mathrm{d}\sigma_{yy}/\mathrm{d}y) = \rho g \cos(\theta). \tag{3.1}$$

The ratio of the shear and normal stresses is a constant in the flow,

$$(\sigma_{xy}/\sigma_{yy}) = -\tan(\theta). \tag{3.2}$$

The energy equation at steady state is

$$\frac{\mathrm{d}}{\mathrm{d}y} K \frac{\mathrm{d}T}{\mathrm{d}y} + \mu\dot{\gamma}^2 - D = 0, \tag{3.3}$$

where K is the thermal conductivity, D is the rate of dissipation of energy, T is the 'granular temperature', μ is the viscosity and $\dot{\gamma}$ is the strain rate, which are specified a little later.

The expressions for the shear and normal stresses depend on the approximation used for the stress tensor. In the Burnett approximation, the shear and normal stresses are given by

$$\sigma_{xy} = \mu\dot{\gamma}, \quad \sigma_{yy} = -p + B\dot{\gamma}^2. \tag{3.4}$$

In the Navier–Stokes approximation, the Burnett coefficient B is set equal to zero. The results of an earlier study on the granular flow of three-dimensional spheres (Kumaran 2006*a*) has shown that there is a significant change in the dependence of density on the angle of inclination when the Burnett term is included in the stress tensor. Consequently, we use the Burnett approximation for the normal stress in the present analysis.

It is convenient to express the viscometric coefficients and the dissipation coefficients as a product of two functions, one of which is a dimensionless function of volume fraction, and the other a product of suitably chosen powers of the granular temperature and particle diameter, the latter having the same dimensions as the viscometric function under consideration. (Note that the granular temperature has dimensions of the square of the velocity, since the mass is set equal to 1.) From dimensional analysis, it can be inferred that pressure is proportional to (T/d^3), μ and K are proportional to $(T^{1/2}/d^2)$, and D is proportional to $(\rho^2 T^{3/2})$, where ρ is the

https://doi.org/10.1017/S002211200700002X Published online by Cambridge University Press

number density, and therefore we write

$$\left.\begin{aligned} &p = p_\phi(T/d^3), \qquad \mu = \mu_\phi(\phi)(T^{1/2}/d^2), \\ &B = B_\phi(\phi)(1/d), \quad K = K_\phi(\phi)(T^{1/2}/d^2), \quad D = D_\phi(\phi)\varepsilon^2(T^{3/2}/d^6), \end{aligned}\right\} \tag{3.5}$$

where the variables with subscript ϕ are dimensionless functions of the volume fraction, and $\varepsilon = (1 - e_n)^{1/2}$ is the small parameter used in the expansion (Kumaran 2004, 2006*a*) to determine the constitutive relations, where e_n is the normal coefficient of restitution. The parameter ε^2 is written separately in the expression for the rate of dissipation of energy in order to ensure that the rate of dissipation goes to zero in the limit of elastic collisions. The strain rate can be expressed in terms of the temperature using (3.4) for the stresses, and (3.2) for the ratio of the stresses,

$$\begin{aligned} \tan(\theta) &= \frac{\mu_\phi(\dot\gamma d/T^{1/2})}{p_\phi - B_\phi(\dot\gamma d/T^{1/2})^2} \\ &= \frac{\mu_\phi G}{p_\phi - B_\phi G^2}. \end{aligned} \tag{3.6}$$

Equation (3.6) is a quadratic equation which can be solved, for a fixed value of $\tan(\theta)$, to obtain the function $G(\phi, \tan(\theta)) = (\dot\gamma d/T^{1/2})$.

It is convenient to scale the y-coordinate by the height of the flowing layer, $y^* = (y/h)$, since this is the length scale for the variation of the potential energy of the particles in the momentum balance equation in the y-direction,

$$\frac{1}{h}\frac{\mathrm{d}}{\mathrm{d}y^*}\left(\frac{(p_\phi - B_\phi G^2)T}{d^3}\right) = \rho g\cos(\theta) = (6/\pi d^3)\phi g\cos(\theta). \tag{3.7}$$

Equation (3.7) indicates that for the pressure to balance the weight per unit area of $O(gh)$, the temperature has to scale as gh in the flowing layer. When the energy balance equation, (3.3), is expressed in terms of the scaled coordinate y^*, we find,

$$(\delta/h)^2\frac{\mathrm{d}}{\mathrm{d}y^*}\left(K_\phi T^{1/2}\frac{\mathrm{d}T}{\mathrm{d}y^*}\right) = -\left(\frac{\mu_\phi G(\phi, \tan(\theta))^2}{\varepsilon^2} - D_\phi\right)T^{3/2}, \tag{3.8}$$

where $\delta = (d/\varepsilon)$ is the 'conduction length' (Kumaran 2004, 2006*a*), and $G(\phi, \tan(\theta))$ is defined in (3.6).

In (3.8), it is apparent that the parameter multiplying the conduction term on the left-hand side is small if the height is large compared to the conduction length, or $h \gg \delta$. This condition is satisfied for the chute flows of Silbert *et al.* (2001). For example, for $h = 40d$, the parameter (δ/h) varies from about 0.08 for $e_n = 0.9$ to about 0.0353 for $e_n = 0.5$. In this case, an asymptotic expansion can be employed and the density and temperature can be expanded in the small parameter δ/h, $\phi = \phi^{(0)} + (\delta/h)\phi^{(1)} + (\delta/h)^2\phi^{(2)}$, with similar expansions for T and G. When these expansions are inserted in the energy equation (3.8), the leading-order equation is

$$\frac{\mu_\phi^{(0)}(G^{(0)})^2}{\varepsilon^2} - D_\phi^{(0)} = 0, \tag{3.9}$$

where we use the notation $\star^{(0)} = \star(\phi)|_{\phi=\phi^{(0)}}$ for the viscosity, thermal conductivity, pressure and rate of dissipation of energy. Equation (3.9) can be solved to obtain the function $G^{(0)}$ as a function of $\phi^{(0)}$,

$$G^{(0)} = \varepsilon(D_\phi^{(0)}/\mu_\phi^{(0)})^{1/2}. \tag{3.10}$$

https://doi.org/10.1017/S002211200700002X Published online by Cambridge University Press

This is inserted into the equation (3.6) for the ratio of the stresses, to obtain

$$\frac{\varepsilon\left(\mu_\phi^{(0)} D_\phi^{(0)}\right)^{1/2}}{p_\phi^{(0)} - \left(B_\phi^{(0)} \varepsilon^2 D_\phi^{(0)} / \mu_\phi^{(0)}\right)} = \tan(\theta). \tag{3.11}$$

In (3.11) the left-hand side is a function the density $\phi^{(0)}$ which is, in general, a function of y, whereas the right-hand side is independent of height. Therefore, the equality in (3.11) can be valid at all values of y only if the leading solution for the volume fraction $\phi^{(0)}$ is independent of y. This density can be explicitly determined as a function of angle θ from a knowledge of the functional forms of $D_\phi^{(0)}$, $\mu_\phi^{(0)}$, B_ϕ and $p_\phi^{(0)}$, as was carried out in an earlier study (Kumaran 2006*a*). An expansion was used in the dense limit, where the pair distribution function is large compared to 1 ($\chi^{(0)} \gg 1$), and the functions $D_\phi^{(0)}$, $p_\phi^{(0)}$, $\mu_\phi^{(0)}$, and $B_\phi^{(0)}$ were expanded in a series in the inverse of the pair correlation function. The leading contributions to these functions are proportional to χ, and so the forms of the expansion correct to $O(\chi^{-1})$ are

$$\left.\begin{aligned} D_\phi^{(0)} &= D_0 \chi^{(0)} + (D_1/\phi^{(0)}) + \left(D_2/{\phi^{(0)}}^2 \chi^{(0)}\right), \\ p_\phi^{(0)} &= p_0 \chi^{(0)} + (p_1/\phi^{(0)}) + \left(p_2/{\phi^{(0)}}^2 \chi^{(0)}\right), \\ \mu_\phi^{(0)} &= \mu_0 \chi^{(0)} + (\mu_1/\phi^{(0)}) + \left(\mu_2/{\phi^{(0)}}^2 \chi^{(0)}\right), \\ B_\phi^{(0)} &= B_0 \chi^{(0)} + (B_1/\phi^{(0)}) + \left(B_2/{\phi^{(0)}}^2 \chi^{(0)}\right). \end{aligned}\right\} \tag{3.12}$$

The above expressions can be obtained from table 1, by expressing ϕ in terms of χ using (2.6) or (2.7) for the pair correlation function. When these expansions are inserted into (3.11), and the left-hand side of (3.11) is expanded in a series in the inverse of the pair correlation function, we obtain an expression of the form

$$\tan(\theta_c) + \frac{C_1}{\phi^{(0)}\chi^{(0)}} + \frac{C_2}{\left(\phi^{(0)}\chi^{(0)}\right)^2} = \tan(\theta) \tag{3.13}$$

where C_0, C_1 and C_2 are determined in terms of the coefficients in (3.12). Equation (3.13) can be solved to obtain $(\phi^{(0)}\chi^{(0)})$ as a function of $\tan(\theta)$, and the volume fraction $\phi^{(0)}$ can be determined from the pair distribution function $\chi^{(0)}$. Once the value of $\phi^{(0)}$ is known, the leading-order temperature field can be determined from the momentum balance equation,

$$T^{(0)} = \frac{6\phi^{(0)} g h (1 - y^*)\cos(\theta)}{\pi(p_\phi^{(0)} - B_\phi^{(0)} G^{(0)2})}. \tag{3.14}$$

Here, we have used the condition that $T^{(0)} = 0$ at the free surface $y^* = (y/h) = 1$ in order to fix the constant in (3.14). Note that it is not possible to apply boundary conditions for the temperature field, since we have neglected the conduction of energy in the leading approximation in (3.8), and converted the equation from a second-order differential equation to a zeroth-order differential equation. The conduction term has to be included in boundary layers at the top and bottom using a theory similar the boundary layer theory for viscous flows, and the boundary layer equations are derived in the next sections.

Next, we turn to the calculation of the higher-order corrections to the volume fraction due to the gradient term on the left-hand side of (3.8). Since the inhomogeneous term is $O(\delta/h)^2$, the first correction to the density $\phi^{(1)}$ is identically equal to zero. The second correction to the density is obtained by substituting the

https://doi.org/10.1017/S002211200700002X Published online by Cambridge University Press

density and temperature expansion into (3.8). The left-hand side of this equation contains only the leading solutions for the density and temperature profiles, while the right-hand side contains terms due to the second corrections to the density and temperature fields. Retaining terms correct to $O(\delta/h)^2$, we obtain

$$\frac{\mathrm{d}}{\mathrm{d}y^*}\left(K_\phi^{(0)}T^{(0)1/2}\frac{\mathrm{d}T^{(0)}}{\mathrm{d}y^*}\right) = -\left(\frac{\mu_\phi G^2}{\varepsilon^2} - D_\phi\right)T^{3/2}\bigg|_2, \tag{3.15}$$

where $K_\phi^{(0)} = K_\phi(\phi^{(0)})$, and the subscript 2 refers to the $O(\delta/h)^2$ contribution to the terms on the right. Since the density-dependent term in brackets on the right-hand side of (3.15) is zero in the leading approximation, and the first corrections to ϕ and T are zero, the $O(\delta/h)^2$ contribution on the right-hand side is given by

$$\left(\frac{\mu_\phi G^2}{\varepsilon^2} - D_\phi\right)T^{3/2}\bigg|_2 = \frac{\mathrm{d}}{\mathrm{d}\phi}\left(\frac{\mu_\phi G^2}{\varepsilon^2} - D_\phi\right)\bigg|_{\phi=\phi^{(0)}}\phi^{(2)}T^{(0)3/2}. \tag{3.16}$$

Using (3.16) for the right-side of (3.15), and inserting the leading-order solution for $T^{(0)}$, we obtain

$$\phi^{(2)} = -\frac{K_\phi^{(0)}}{2(1-y^*)^2}\left(\frac{\mathrm{d}}{\mathrm{d}\phi}\left(\frac{\mu_\phi G^2}{\varepsilon^2} - D_\phi\right)\bigg|_{\phi=\phi^{(0)}}\right)^{-1}. \tag{3.17}$$

To summarize, we have used an asymptotic analysis in the small parameter (δ/h) to show that the volume fraction in the bulk of the flow is a constant in the leading approximation, and the correction to the volume fraction is $(\delta/h)^2\phi^{(2)}$, where $\phi^{(2)}$ is given in (3.17). The parameter (δ/h) was earlier estimated for $h = 40d$, for the smallest values of h used in the simulations of Silbert *et al.* (2001) as varying between 0.08 for $e_n = 0.9$ and 0.0353 for $e_n = 0.5$. Consequently, the correction to the volume fraction is expected to vary between $0.0064\phi^{(2)}$ for $e_n = 0.9$ and $0.00125\phi^{(2)}$ for $e_n = 0.5$.

The numerical results for $(\phi^{(2)}(1-y^*)^2)$ as a function of volume fraction are shown in figure 2 for the rough nearly elastic particle models, and in figure 3 for the partially rough inelastic particle model. The coefficients for the pressure, viscosity, conductivity and Burnett coefficient from table 1 are used, and results are shown for the Carnahan–Starling pair distribution (equation (2.6)) and the high-density pair distribution (equation (2.7)). It is observed that $(\phi^{(2)}(1-y^*)^2)$ has a maximum value of about 2 near close packing for rough nearly elastic particles. The value of $\phi^{(2)}$ increases at lower volume fractions and it diverges at a volume fraction close to 0.1 because the denominator (last term on the right-hand side of (3.17)) passes through zero, but such low volume fractions are not encountered in practical applications or in the simulations (Silbert *et al.* 2001). This indicates that the variation in volume fraction is, at most, about 1.2 % even for thin layers of thickness 40 particle diameters and $e_n = 0.9$, for which $(\delta/h)^2 = 0.0064$, when the volume fraction is greater than about 0.3 in three dimensions, and the variation decreases as the collisions become more inelastic. These variations may be difficult to observe in graphs of simulation results, since they are smaller than the typical symbol size or error bar in the graph.

An example of the density profile predicted by the above analysis, for $\phi^{(0)} = 0.60$ and for different coefficients of restitution, is shown for a layer with thickness 40 particle diameters in figure 4. It is observed that the density profile is remarkably constant between $e_n = 0.5$ and $e_n = 0.9$, though this solution is not valid within boundary layers of thickness about 5 particle diameters at the top and bottom as noted earlier. The density profile does show some variation for $e_n = 0.98$ because the parameter (δ/h)

https://doi.org/10.1017/S002211200700002X Published online by Cambridge University Press

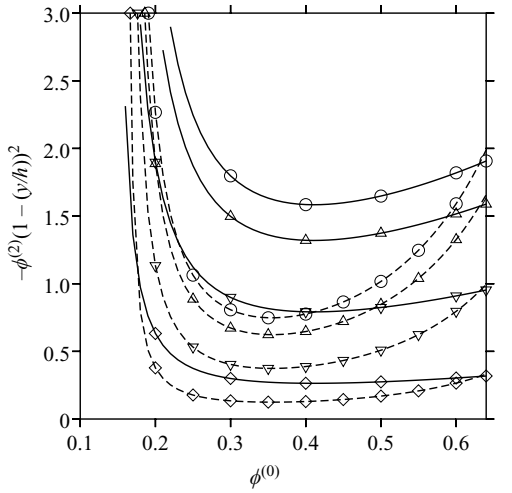


FIGURE 2. The parameter $(\phi^{(2)}(1-(y/h))^2)$ (equation (3.17)) as a function of $\phi^{(0)}$ for the rough nearly elastic model with $a_t = 0\,(\bigcirc)$, $a_t = 0.2\,(\triangle)$, $a_t = 1.0\,(\nabla)$, $a_t = 5.0\ (\diamond)$. The broken lines show the results when the pair distribution function is given by the Carnahan–Starling equation of state (equation (2.6)), and the solid lines show the results when the pair distribution function is given by the high-density equation of state (equation (2.7)).

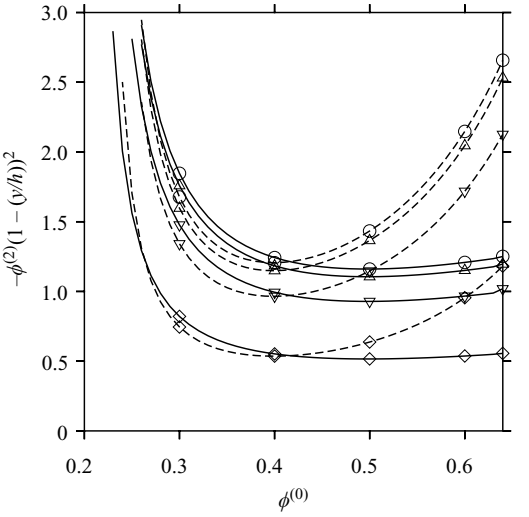


FIGURE 3. As figure 2 but for the partially rough nearly elastic model.

is 0.177, and is no longer small, but even this variation is small in the centre of the layer. The simulations of Silbert *et al.* (2001) show an example of a profile at $e_n = 0.98$ which looks much flatter than figure 2, but it should be noted that Silbert *et al.* had a non-zero friction coefficient, which would result in a larger energy dissipation than that for frictionless particles with $e_n = 0.98$. Thus, the present analysis captures the remarkable lack of observable variation of the volume fraction with height, and with angle of inclination near close packing.

It is observed, in figures 2 and 3, that $\phi^{(2)}$ diverges as the coefficient of restitution is decreased, because the derivative with respect to volume fraction in (3.17) passes

https://doi.org/10.1017/S002211200700002X Published online by Cambridge University Press

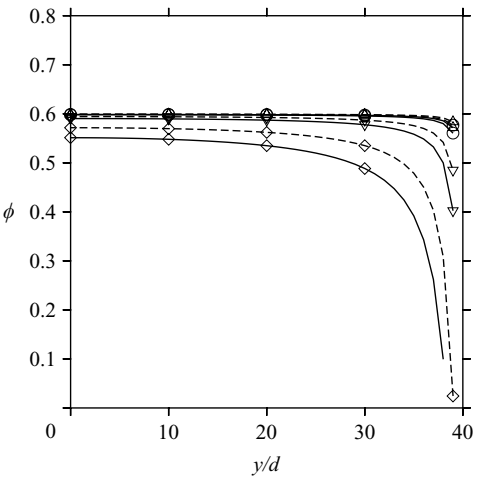


FIGURE 4. Volume fraction ϕ as a function of the ratio of the height and particle diameter, (y/d), for the rough nearly elastic model (solid line); the partially rough nearly elastic model (dashed line) with $a_t = 1.0$, for $h = 40d$, $e_n = 0.5$, $\theta = 22.00^o$ ($\bigcirc$), $h = 40d$, $e_n = 0.7$, $\theta = 21.05^o$ ($\triangle$), $h = 40d$, $e_n = 0.9$, $\theta = 19.23^o$ ($\triangledown$) and $h = 40d$, $e_n = 0.98$, $\theta = 11.01^o$ ($\diamond$). The pair distribution function was assumed to be the high-density equation of state (equation (2.7)) in all cases.

through zero. This suggests that for the models used here, there is a range of coefficients of restitution where a steady flow is not possible. The absence of a solution for certain parameter values was also noted by Louge (2003). This is the result of the fact that at low volume fractions, the derivative with respect to volume fraction in (3.17) is negative, whereas it becomes positive at high volume fraction for the models considered here, and passes through zero at an intermediate value of the volume fraction. The divergence could be avoided if the next higher term in the expansion, which is proportional to the second derivative of the difference between production and dissipation with respect to volume fraction, were included in (3.16) in the volume fraction range where the first derivative passes through zero. However, it should be noted that the divergence occurs at a relatively small value of the volume fraction, in the range $\phi^{(0)} = 0.2 - 0.3$, which is not relevant for the dense flows considered here. Therefore, we do not refine the theory further.

4. Boundary layer solution at the bottom surface

The leading-order solution (3.14) cannot satisfy the boundary conditions at the top and bottom surfaces, because the rate of conduction of energy is neglected in comparison to the rate of production and dissipation, thereby converting the second-order differential equation to an algebraic equation. Within distances comparable to the conduction length from the boundaries, it is necessary to rescale the y-coordinate by the conduction length $\delta = (d/\varepsilon)$. The 'inner' coordinate near the bottom surface is defined as $y^\dagger = (y/\delta)$. In this and the following sections, we refer to the leading-order volume fraction in the bulk flow as ϕ_o, and use the symbols ϕ and T for the volume fraction and temperature in the boundary layer. The y momentum equation and the

https://doi.org/10.1017/S002211200700002X Published online by Cambridge University Press

energy equation can be written in terms of the inner coordinate $y^\dagger$ as

$$\frac{\mathrm{d}((p_\phi - B_\phi G)T)}{\mathrm{d}y^\dagger} = -\frac{6\phi g\delta\cos(\theta)}{\pi}, \tag{4.1}$$

$$\frac{\mathrm{d}}{\mathrm{d}y^\dagger}K_\phi T^{1/2}\frac{\mathrm{d}T}{\mathrm{d}y^\dagger} = -T^{3/2}\left(\frac{\mu_\phi G(\phi,\tan(\theta))^2}{\varepsilon^2} - D_\phi\right), \tag{4.2}$$

where p_ϕ, K_ϕ, μ_ϕ and D_ϕ are defined in (3.5). In the momentum conservation equation (4.1), the left-hand side scales as (gh), since the temperature is proportional to (gh), while the right-hand side scales as $(g\delta)$. Therefore, in an asymptotic expansion in the parameter (δ/h), the right-hand side of (4.1) can be neglected in comparison to the left-hand side. The leading-order momentum equation is given by

$$\frac{\mathrm{d}((p_\phi - B_\phi G^2)T)}{\mathrm{d}y^\dagger} = 0. \tag{4.3}$$

If the leading-order equation were solved in a naive manner, the solution would turn out to be

$$T = \frac{\phi_o gh\cos(\theta)}{(p_\phi - B_\phi G^2)} \tag{4.4}$$

where the constant of integration on the right-hand side is determined from the pressure in the limit $y \to 0$ in the outer solution. However, it should be noted that this solution does not match with the outer solution (3.14) in the limit $y^\dagger \to \infty$ and $y^* \to 0$, and we shall use the matching conditions to modify the solution (4.4) a little later.

The spatial evolution equation for the volume fraction is obtained by inserting the expressions for the temperature (4.4) into the energy conservation equation (4.2),

$$\frac{\mathrm{d}}{\mathrm{d}y^\dagger}\left(-\frac{(p_\phi - B_\phi G^2)' K_\phi}{(p_\phi - B_\phi G^2)^{5/2}}\frac{\mathrm{d}\phi}{\mathrm{d}y^\dagger}\right) = -\frac{1}{(p_\phi - B_\phi G^2)^{3/2}}\left(\frac{\mu_\phi G(\phi,\tan(\theta))^2}{\varepsilon^2} - D_\phi\right) \tag{4.5}$$

where primes denote derivatives with respect to ϕ. Equation (4.5) can be simplified to obtain a second-order differential equation for ϕ,

$$\frac{\mathrm{d}^2\phi}{\mathrm{d}y^{\dagger 2}} + E(\phi)\left(\frac{\mathrm{d}\phi}{\mathrm{d}y^\dagger}\right)^2 = F(\phi) \tag{4.6}$$

where

$$\left.\begin{aligned} E(\phi) &= \frac{(p_\phi - B_\phi G^2)^{5/2}}{(p_\phi - B_\phi G^2)' K_\phi}\left(\frac{(p_\phi - B_\phi G^2)' K_\phi}{(p_\phi - B_\phi G^2)^{5/2}}\right)', \\ F(\phi) &= \frac{p_\phi - B_\phi G^2}{(p_\phi - B_\phi G^2)' K_\phi}\left(\frac{\mu_\phi G(\phi,\tan(\theta))^2}{\varepsilon^2} - D_\phi\right). \end{aligned}\right\} \tag{4.7}$$

Equation (4.6) is a nonlinear equation, which has to be solved for a specific model for the pressure, viscosity and thermal conductivity, in order to obtain the volume fraction as a function of height in the boundary layer. It is also a second-order differential equation in $y^\dagger$, which requires two boundary conditions. One of these is the matching condition in the limit $y^\dagger \to \infty$,

$$\phi \to \phi_o \text{ for } y^\dagger \to \infty. \tag{4.8}$$

The second is the condition for either the temperature or the flux at the base. The Jenkins & Richman (1985) conditions at the bottom surface balance the heat

https://doi.org/10.1017/S002211200700002X Published online by Cambridge University Press

flux towards the base J with the rate of dissipation of energy D. Since the heat flux, $-K(\mathrm{d}T/\mathrm{d}z)$, where K is $T^{1/2}$ times a function of volume fraction, and D is proportional to $T^{3/2}$, the Jenkins & Richman conditions have the form

$$\frac{\mathrm{d}T}{\mathrm{d}y} = \beta T \tag{4.9}$$

where β is a positive function of the volume fraction at the base when the base is dissipative. If there is an energizing base which supplies energy to the flow, the function β is negative, and the temperature decreases with an increase in height from the surface. It is also possible to consider other boundary conditions, such as a constant temperature or a constant heat flux at the surface. However, before imposing boundary conditions, we first examine whether solutions exist for (4.6) in the limit $y^\dagger \to \infty$.

Equation (4.6) is most conveniently expressed in terms of the departure from the volume fraction ϕ_o in the outer layer,

$$\frac{\mathrm{d}^2(\phi-\phi_o)}{\mathrm{d}y^{\dagger 2}} + E(\phi)\left(\frac{\mathrm{d}(\phi-\phi_o)}{\mathrm{d}y^\dagger}\right)^2 = F(\phi). \tag{4.10}$$

For $\phi \to \phi_o$, (4.10) can be linearized in the difference $(\phi-\phi_o)$ about $\phi=\phi_o$. It should be noted that $F(\phi_o)=0$ for the outer solution from (3.9), and therefore $F(\phi)$ can be approximated as $(\mathrm{d}F(\phi)/\mathrm{d}\phi)|_{\phi=\phi_o}(\phi-\phi_o)$. The resulting linear equation is

$$\frac{\mathrm{d}^2(\phi-\phi_o)}{\mathrm{d}y^{\dagger 2}} = H(\phi_o)(\phi-\phi_o) \tag{4.11}$$

where

$$H(\phi_o) = \left.\frac{\mathrm{d}F(\phi)}{\mathrm{d}\phi}\right|_{\phi=\phi_o}. \tag{4.12}$$

The solution of this equation, consistent with the requirement that the perturbation to the volume fraction should be finite for $y^\dagger \to \infty$, is

$$\phi = \phi_o + C\exp(-\sqrt{H(\phi_o)}\,y^\dagger) \tag{4.13}$$

where C is a constant to be determined from the boundary conditions. Clearly, exponentially decaying solutions which satisfy the matching condition for $y^\dagger \to \infty$ exist only if $H(\phi_o)$ is positive. If $H(\phi_o)$ is negative, there are no solutions that satisfy the boundary condition for $y^\dagger \to \infty$. Thus, a boundary layer solution for the energy field requires that $H(\phi)$ is positive at $\phi=\phi_o$.

The function $H(\phi_o)$ is shown as a function of the coefficient of restitution for different volume fractions in figure 5 for the rough particle model, and in figure 6 for the partially rough particle model. The function $H(\phi_o)$ has some common features for both the rough and partially rough particle models. It is observed that $H(\phi_o)$ is negative when the coefficient of restitution is very close to 1, indicating that a boundary layer solution cannot be obtained in the limit of elastic inter-particle collisions. However, $H(\phi_o)$ changes sign and assumes positive values as the coefficient of restitution decreases in all cases. This implies that an exponentially decreasing boundary layer solution exists when the coefficient of restitution is less than a maximum value for both the rough and partially rough particle models, and a boundary layer solution does not exist when the coefficient of restitution increases beyond this value. Figures 7 and 8 show the contours in the $\phi_o - e_n$ plane separating regions where a boundary layer solution does and does not exist. A boundary layer

https://doi.org/10.1017/S002211200700002X Published online by Cambridge University Press

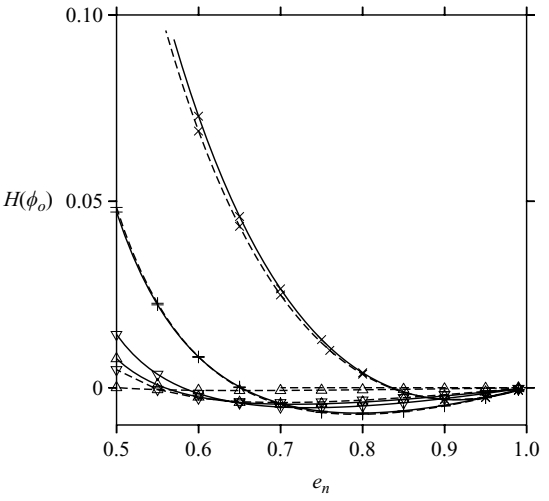


FIGURE 5. The function $H(\phi_o)$ (equation (4.12)) as a function of e_n for the rough particle model with $a_t = 0$, and $\phi_o = 0.64$ ($\triangle$), $\phi_o = 0.6$ ($\triangledown$), $\phi_o = 0.5$ (+), $a_t = 0.3$ ($\times$). The solid lines show the results when the pair distribution function is given by the Carnahan–Starling equation of state (equation (2.6)), and the broken lines show the results when the pair distribution function is given by the high-density equation of state (equation (2.7)).

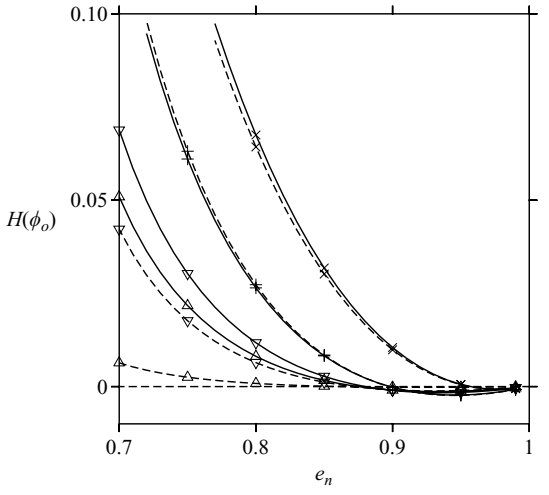


FIGURE 6. As figure 5 but for the partially rough particle model.

solution does exist for parameter values below the lines shown in figures 7 and 8. It is observed that the boundary layer solution exists over a much larger range of coefficients of restitution for the partially rough particle model, and a relatively smaller range for the rough particle model, for the forms of the pair correlation function used here.

Thus, the above analysis indicates that a boundary layer solution does not exist under all conditions, but only for specific parameter values. In particular, there is a critical dependence on the variation of the parameter $(\mu_\phi G(\phi, \tan(\theta))^2/\varepsilon^2 - D_\phi)$ with ϕ about $\phi = \phi_o$, and it is necessary to evaluate this parameter in order to assess whether a boundary layer solution is possible or not. This is in contrast to viscous

https://doi.org/10.1017/S002211200700002X Published online by Cambridge University Press

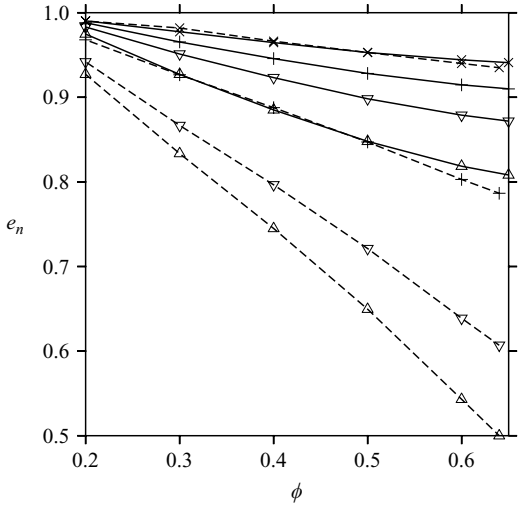


FIGURE 7. Contours in the $\phi_o - e_n$ plane where $H(\phi_o) = 0$ for the rough particle model for $a_t = 0$ ($\triangle$), $a_t = 0.2$ ($\triangledown$), $a_t = 1.0$ ($+$), $a_t = 5.0$ ($\times$). A boundary layer solution that decreases exponentially into the bulk exists below the lines shown in the figure.

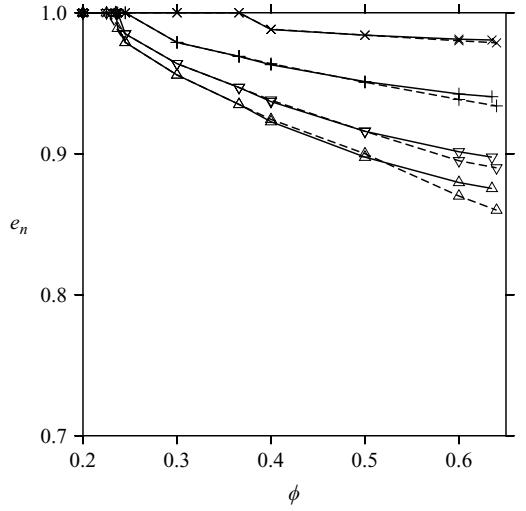


FIGURE 8. As figure 7 but for the partially rough particle model.

boundary layer solutions in high-Reynolds-number fluids flows, for example, which always exist. However, it is still necessary to solve a nonlinear equation, (4.10), in order to obtain the actual volume fraction and temperature profiles in the boundary layer. There are difficulties with existence and uniqueness due to the nonlinear nature of the equation. There is an additional complication, which is the rapid variation of the pair distribution function with volume fraction as the limit of close packing is approached. In the following analysis, we attempt to get around this difficulty by using the pair distribution function, rather than the volume fraction, as the fundamental variable. For the purpose of calculation, we use the high-density pair distribution function (2.7), and we invert this pair distribution function in order to express the volume fraction in terms of the pair distribution function.

https://doi.org/10.1017/S002211200700002X Published online by Cambridge University Press

For a dense granular flow, the pair distribution function is numerically large, and an expansion can be used in the inverse of the pair distribution function, χ^{-1}. The leading-order terms in the expansion are retained to obtain an analytical solution for the variation of the density with height. Since the functions p_ϕ, μ_ϕ, K_ϕ and D_ϕ diverge proportionally to χ in this limit, it is convenient to express the viscometric parameters and the dissipation rate as

$$\left.\begin{aligned} p &= (p_c T \chi/d^3), \quad K = (K_c T^{1/2}\chi/d^2), \quad \mu = (\mu_c T^{1/2}\chi/d^2), \\ B &= (B_c \chi/D), \quad D = (D_c \varepsilon^2 T^{3/2}\chi/d^4), \quad G = G_c, \end{aligned}\right\} \tag{4.14}$$

where G_c is obtained in terms of p_c, μ_c, B_c and $\tan(\theta)$ using (3.6). A similar truncation is not sufficient for the inhomogeneous term on the right-hand side of (4.2), since it is zero in the leading approximation in the high-density limit. It is convenient to rewrite the right-hand side of (4.5) as

$$-T^{3/2} D_\phi \left(\frac{\mu_\phi G(\phi, \tan(\theta))^2}{D_\phi \varepsilon^2} - 1 \right). \tag{4.15}$$

The ratio $(\mu_\phi G(\phi, \tan(\theta))^2/D_\phi\varepsilon^2)$ tends to a constant for $\chi \gg 1$ in the close packing limit, since μ_ϕ and D_ϕ are proportional to χ in this limit, while $G(\phi, \tan(\theta))$ tends to a constant. Therefore, (4.15) has the form

$$T^{3/2} D_\phi \left(R_c' + \frac{R_c}{\chi} - 1 \right) \tag{4.16}$$

correct to $O(\chi^{-1})$, where R_c' and R_c are constants. In addition, $(\mu_\phi G(\phi, \tan(\theta))^2/D_\phi\varepsilon^2)$ is identically equal to 1 for the outer solution $\phi = \phi_o$, or $\chi = \chi_o$, where χ_o is the pair distribution function in the outer region. Therefore, $(R_c' - 1) = -(R_c/\chi_o)$ in (4.16), and the right-hand side of (4.5) is

$$T^{3/2} D_c \chi R_c \left(\frac{1}{\chi} - \frac{1}{\chi_o} \right). \tag{4.17}$$

A relation between the parameter R_c in (4.15) and (4.16), and the parameter $H(\phi_o)$ in (4.12), can be obtained as follows. Note that the parameter R_c can also be expressed as the negative of the derivative of $(\mu_\phi G(\phi, \tan(\theta))^2/D_\phi)$ with respect to χ^{-1}, at $\chi = \chi_o$,

$$\begin{aligned} R_c &= -\frac{\mathrm{d}}{\mathrm{d}\chi^{-1}} \left(\frac{\mu_\phi G(\phi, \tan(\theta))^2}{D_\phi} \right)\Bigg|_{\chi=\chi_o} \\ &= \chi^2 \frac{\mathrm{d}}{\mathrm{d}\chi} \left(\frac{\mu_\phi G(\phi, \tan(\theta))^2}{D_\phi} \right)\Bigg|_{\chi=\chi_o}. \end{aligned} \tag{4.18}$$

The function $H(\phi_o)$ in (4.12) can be expressed as

$$\begin{aligned} H(\phi_o) &= \frac{\mathrm{d}}{\mathrm{d}\phi} \left(\frac{(p_\phi - B_\phi G^2) D_\phi}{(p_\phi - B_\phi G^2)' K_\phi} \left(\frac{\mu_\phi G(\phi, \tan(\theta)^2)}{D_\phi \varepsilon^2} - 1 \right) \right)\Bigg|_{\phi=\phi_o} \\ &= \frac{\mathrm{d}}{\mathrm{d}\chi} \left(\frac{(p_\phi - B_\phi G^2) D_\phi}{(p_\phi - B_\phi G^2)' K_\phi} \left(\frac{\mu_\phi G(\phi, \tan(\theta)^2)}{D_\phi \varepsilon^2} - 1 \right) \right) \times \frac{\mathrm{d}\chi}{\mathrm{d}\phi}\Bigg|_{=\phi_o} \\ &= \frac{(p_\phi - B_\phi G^2) D_\phi}{(p_\phi - B_\phi G^2)' K_\phi} \frac{\mathrm{d}}{\mathrm{d}\chi} \left(\frac{\mu_\phi G(\phi, \tan(\theta)^2)}{D_\phi \varepsilon^2} - 1 \right) \times \frac{\mathrm{d}\chi}{\mathrm{d}\phi}\Bigg|_{=\phi_o}. \end{aligned} \tag{4.19}$$

https://doi.org/10.1017/S002211200700002X Published online by Cambridge University Press

The final simplification in (4.19) can be made because $((\mu_\phi G(\phi, \tan(\theta))/D_\phi \varepsilon^2) - 1) = 0$ at $\phi = \phi_o$. Therefore, $H(\phi_o)$ can be written in terms of R_c as

$$H(\phi_o) = \frac{R_c}{\chi^2} \frac{(p_\phi - B_\phi G^2) D_\phi}{(p_\phi - B_\phi G^2)' K_\phi} \frac{\mathrm{d}\chi}{\mathrm{d}\phi}\bigg|_{\phi=\phi_o}. \tag{4.20}$$

In (4.20) note that $(p_\phi - B_\phi G^2)$ is the negative of the normal stress, which has to be positive in the boundary layer in order to support the weight of material above. In addition, the derivative of the normal stress with volume fraction should also be positive for stability. Since all terms in (4.20) except R_c are positive, it follows that $H(\phi_o)$ is positive if R_c is positive. Thus, the domains of positive $H(\phi_o)$ in figures 5 and 6 correspond to the domains of positive R_c.

With the simplifications for the viscometric parameters in (4.14), and the simplification for the difference between rates of shear production and inelastic dissipation in (4.17), the momentum and energy equations (4.3) and (4.5) can be written as

$$T = \frac{6\phi_o g h \cos(\theta)}{\pi(p_c - B_c G_c^2)\chi}, \tag{4.21}$$

$$\frac{\mathrm{d}}{\mathrm{d}y^\dagger} K_c \sqrt{\chi} \frac{\mathrm{d}(\chi)^{-1}}{\mathrm{d}y^\dagger} = \frac{D_c R_c}{\sqrt{\chi}} \left(\frac{1}{\chi} - \frac{1}{\chi_o} \right). \tag{4.22}$$

It is convenient to express (4.22) in terms of the dimensionless parameter $\psi = (\chi/\chi_o)^{-1/2}$. Equation (4.22) then becomes

$$2\frac{\mathrm{d}^2\psi}{\mathrm{d}y^{\dagger 2}} = \frac{R_c D_c}{\chi_o K_c}(\psi^3 - \psi). \tag{4.23}$$

This equation can easily be solved, subject to the boundary condition $(\mathrm{d}\psi/\mathrm{d}y) \to 0$ and $\psi \to 1$ in the limit $y \to \infty$, to obtain

$$\psi = \frac{1 - c\exp(-\alpha y^\dagger)}{1 + c\exp((-\alpha y^\dagger)} \tag{4.24}$$

where $\alpha^2 = (R_c D_c / 2K_c \chi_o)$, and c is the constant of integration to be determined from the boundary conditions. The temperature can be easily determined using (4.4) and (4.14), where $\chi = (\chi_o/\psi^2)$, and ψ is given by (4.24),

$$T = \frac{6\phi_o g h \cos(\theta)}{\pi(p_c - B_c G_c^2)\chi_o} \left(\frac{1 - c\exp(-\alpha y^\dagger)}{1 + c\exp(-\alpha y^\dagger)} \right)^2. \tag{4.25}$$

A uniform solution is obtained by asymptotic matching of (4.25), which is valid in the boundary layer, with (3.14), which is valid in the bulk of the flow. In the asymptotic matching procedure, the inner and outer solutions are added together, and the common limiting value of the outer solution (in the limit $y^* \to 0$) and the inner solution (in the limit $y^\dagger \to \infty$) is subtracted, to obtain

$$T = \frac{6\phi_o g \cos(\theta)}{\pi p_c \chi_o} \left(h \left(\frac{1 - c\exp(-\alpha y^\dagger)}{1 + c\exp(-\alpha y^\dagger)} \right)^2 - y \right). \tag{4.26}$$

https://doi.org/10.1017/S002211200700002X Published online by Cambridge University Press

Next, we determine the constant c from the boundary conditions. The temperature and the temperature gradient at $y^\dagger = 0$ are given by

$$\left.\begin{aligned} T &= \frac{6\phi_o g h \cos(\theta)}{(p_c - B_c G_c^2)\chi_o}\left(\frac{1-c}{1+c}\right)^2, \\ \frac{\mathrm{d}T}{\mathrm{d}y} &= \frac{6\phi_o g h \cos(\theta)}{\pi(p_c - B_c G_c^2)\chi_o}\frac{4\alpha(1-c)c}{\delta(1+c)^3}. \end{aligned}\right\} \tag{4.27}$$

With the above expressions for the temperature and temperature gradient, the Jenkins–Richman boundary conditions reduce to the form

$$\frac{4\alpha c}{\delta(1-c^2)} = \beta. \tag{4.28}$$

Thus, the solution for the constant c is

$$c = -\frac{2\alpha}{\delta\beta} \pm \frac{\sqrt{4\alpha^{\dagger 2} + \delta^2\beta^2}}{\delta\beta}. \tag{4.29}$$

The positive or negative sign to be used in (4.29) can be inferred from (4.27) for the temperature. This equation indicates that for c greater than $+1$ or c less than -1, the temperature is either zero or infinity at some point in the boundary layer. Since this is unphysical, it is necessary that c be bounded between -1 and $+1$. This requires that the positive sign be used in (4.29) for $\beta > 0$, and the negative sign be used for $\beta < 0$.

A brief digression is made in order to derive a significant relationship between the existence of a boundary layer solution derived in the present section, and the existence of a flow in which the volume fraction decreases as the angle of inclination decreases as derived in an earlier study (Kumaran 2006*a*). The following theorem is proved:

THEOREM 1. *A boundary layer solution at the bottom boundary for the flow down an inclined plane exists if and only if the volume fraction in the bulk decreases as the angle of inclination is increased.*

In Kumaran (2006*a*), the volume fraction was related to the angle of inclination using (3.6), where $G = (d\dot{\gamma}/T^{1/2})$. For later convenience, we refer to the right-hand side of (3.6) as $P(\phi, G)$:

$$P(\phi, G) = \frac{\mu_\phi G}{p_\phi - B_\phi G^2}. \tag{4.30}$$

The parameter G, which provides the relation between the strain rate and the temperature, was obtained from the balance between the rates of production and dissipation of energy. It is convenient to work with the function $Q(\phi, G)$, which is defined as the difference between the (ratio of the rates of production and dissipation) and 1, which has to be zero,

$$Q(\phi, G) = \left(\frac{\mu_\phi G^2}{D_\phi \varepsilon^2} - 1\right) = 0. \tag{4.31}$$

Equation (4.31) is used to obtain G in terms of the volume fraction, and inserted into (4.30), to obtain the angle of inclination as a function of volume fraction. In Kumaran (2006*a*), a flow was considered to be physically realistic if the volume fraction decreases as the angle of inclination increases. This requires that the derivative of $P(\phi, G)$ with respect to ϕ *at constant* $Q(\phi)$ has to be negative. Therefore, the volume fraction

https://doi.org/10.1017/S002211200700002X Published online by Cambridge University Press

decreases as the angle of inclination increases only for

$$\left.\frac{\partial P(\phi, G)}{\partial \phi}\right|_{Q(\phi,G)=0} < 0. \tag{4.32}$$

In the present boundary layer analysis, we showed that a boundary layer solution exists only for

$$H(\phi) = \frac{(p_\phi - B_\phi G^2) D_\phi}{(p_\phi - B_\phi G^2)' K_\phi} \left.\frac{\mathrm{d}}{\mathrm{d}\phi}\left(\frac{\mu_\phi G(\phi, \tan(\theta)^2)}{D_\phi \varepsilon^2} - 1\right)\right|_\phi > 0. \tag{4.33}$$

Note that $H(\phi)$ can be written in terms of the derivative of the function $Q(\phi, G)$ with respect to ϕ,

$$H(\phi) = \frac{(p_\phi - B_\phi G^2) D_\phi}{(p_\phi - B_\phi G^2)' K_\phi} \left.\frac{\mathrm{d}Q}{\mathrm{d}\phi}\right|_{P(G,\phi)=\tan(\theta)}, \tag{4.34}$$

and $H(\phi)$ is positive when $(\mathrm{d}Q/d\phi)|_{P(G,\phi)=\tan(\theta)}$ is positive. Therefore, boundary layer solutions exist only when

$$\left.\frac{\mathrm{d}Q}{\mathrm{d}\phi}\right|_{P(G,\phi)=\tan(\theta)} > 0. \tag{4.35}$$

Next, (4.32) and (4.35) are compared, using the identity

$$\left.\frac{\mathrm{d}P}{\mathrm{d}Q}\right|_\phi \left.\frac{\partial Q}{\partial \phi}\right|_P = -\left.\frac{\mathrm{d}P}{\mathrm{d}\phi}\right|_Q. \tag{4.36}$$

The derivative $(\mathrm{d}Q/\mathrm{d}P)|_\phi$ can be evaluated by first substituting for G in terms of Q from (4.31), and then inserting this into (4.30),

$$\begin{aligned}\left.\frac{\mathrm{d}P}{\mathrm{d}Q}\right|_\phi &= \left.\frac{\mathrm{d}}{\mathrm{d}Q}\left(\frac{\sqrt{\mu D_\phi \varepsilon^2 (Q+1)}}{p_\phi - (B_\phi D_\phi \varepsilon^2 (Q+1)/\mu_\phi)}\right)\right|_\phi \\ &= \frac{\sqrt{\mu_\phi D_\phi \varepsilon^2}}{2\sqrt{Q+1}}\left(\frac{p_\phi + (B_\phi D_\phi \varepsilon^2/\mu_\phi)(Q+1)}{(p_\phi - (B_\phi D_\phi \varepsilon^2/\mu_\phi)(Q+1))^2}\right).\end{aligned} \tag{4.37}$$

Since the above derivative is taken for a state where there is a balance between production and dissipation in the bulk, $Q(\phi, G)$ in (4.31) is zero, and the derivative $(\mathrm{d}P/\mathrm{d}Q)|_\phi$ is always positive in (4.37). Therefore, (4.36) indicates that conditions (4.32) and (4.35) are either satisfied simultaneously, or are violated simultaneously. This proves the theorem that a boundary layer solution at the bottom surface for the flow down an inclined plane exists if and only if the volume fraction in the bulk decreases as the angle of inclination is increased.

It should be noted that the above result is derived for the existence of a solution, and not for its stability; a more detailed stability analysis would be required to analyse the stability about the base state. The result is general, in the sense that it is valid for all models for which the bulk flow and the boundary layer are described by the same constitutive relations for the stress and energy flux, and the same stress ratio and energy balance conditions are used in the boundary layer and the bulk.

https://doi.org/10.1017/S002211200700002X Published online by Cambridge University Press

5. Boundary layer solution at top surface

As the top surface is approached from below, there is a transition from a dense collisional flow to a dilute regime in which the particle motion is ballistic. Simulations show that there is a deviation from the linear temperature profile to a profile which seems to approach a constant value, or shows an increase, as the top surface is approached. In addition, the volume fraction decreases sharply from its constant value near the top surface. In simulations, the length scale for the deviation of the temperature from its linear form is larger than the length scale for the decrease in the density. In this analysis, scaling arguments are used to show that the length scale over which the density decreases is (δ/χ_o), which is much smaller than the conduction length δ for temperature variations in the dense limit where $\chi_o \gg 1$. We use this separation of scales, along with asymptotic matching, in order to construct a boundary layer theory for the evolution of the temperature and density at the top surface. As in the previous section, two parameters are used in the asymptotic analysis: the ratio of the conduction length and the height of the flowing layer, (δ/h), which is small compared to 1, and the pair distribution function at contact in the bulk, χ_o, which is large compared to 1. In the following analysis, we first assume that the density decreases sharply over a distance small compared to that for the temperature evolution from its linear value, and show at the end of this section that the assumption is self-consistent.

In order to analyse the boundary layer, we choose the origin of the coordinate system at the location where the density profile decreases sharply to zero, and choose the coordinate $Y = (h - y)$, so that Y is positive into the granular layer, as shown in figure 1. Since the length scale for the density decrease is small compared to that for the variation of temperature, we assume that the density profile is a step function at $Y = 0$. Since the pair correlation function χ is large compared to 1 in the boundary layer, we can use the approximation (4.14) for the y-momentum balance equation,

$$\frac{\mathrm{d}(\chi T)}{\mathrm{d}Y} = \frac{6\phi_c g \cos(\theta)}{\pi(p_c - B_c G_c^2)}. \tag{5.1}$$

This can be easily solved to obtain

$$T = \frac{6\phi_c g Y \cos(\theta)}{\pi(p_c - B_c G_c^2)\chi}. \tag{5.2}$$

The energy conservation equation (3.8), expressed in terms of T and Y, using the approximation (4.17) for the right-hand side of the energy balance equation, is

$$\frac{\mathrm{d}}{\mathrm{d}Y}\left(\frac{K_c\chi}{d^2}T^{1/2}\frac{\mathrm{d}T}{\mathrm{d}Y}\right) = \frac{D_c\varepsilon^2\chi}{d^4}T^{3/2}R_c\left(\frac{1}{\chi} - \frac{1}{\chi_o}\right). \tag{5.3}$$

Using the substitution (5.2) for the temperature, we obtain a second-order differential equation for χ,

$$\frac{\mathrm{d}}{\mathrm{d}Y}\left(\chi^{1/2}Y^{1/2}\frac{\mathrm{d}(Y/\chi)}{\mathrm{d}Y}\right) = \frac{D_c R_c}{K_c\delta^2}\frac{Y^{3/2}}{\chi^{1/2}}\left(\frac{1}{\chi} - \frac{1}{\chi_o}\right). \tag{5.4}$$

Using the substitution $\psi = (\chi/\chi_o)^{-1/2}$, we obtain an equation for ψ,

$$\frac{\mathrm{d}^2\psi}{\mathrm{d}Y^{\dagger 2}} + \frac{2}{Y^\dagger}\frac{\mathrm{d}\psi}{\mathrm{d}Y^\dagger} + \frac{\psi}{4Y^{\dagger 2}} = \alpha^2(\psi^3 - \psi) \tag{5.5}$$

where the scaled distance $Y^\dagger = (Y/\delta)$, and the parameter $\alpha^2 = (R_c D_c/2K_c\chi_o)$. It is necessary to solve this equation subject to the boundary condition $\psi = 1(\chi = \chi_o)$ in

https://doi.org/10.1017/S002211200700002X Published online by Cambridge University Press

the limit $Y^\dagger \to \infty$, and a matching condition for the energy flux at $Y^\dagger = 0$ which will be determined a little later.

It is difficult to solve (5.5) analytically, and before proceeding to solve it numerically, it is instructive to examine the limiting behaviour of the solutions. In the limit $Y^\dagger \to 0$, there are two linearly independent solutions for ψ,

$$\psi_1 = C(\alpha Y^\dagger)^{-1/2} + C^3(\alpha Y^\dagger)^{1/2} + o(Y^{\dagger 1/2}), \tag{5.6}$$

$$\psi_2 = D\log(\alpha Y^\dagger)(\alpha Y^\dagger)^{-1/2} + D^3(\log(\alpha Y^\dagger)^3 - 6\log(\alpha Y^\dagger)^2 + 18\log(\alpha Y^\dagger) - 24)(\alpha Y^\dagger)^{1/2} + O(Y^{\dagger 1/2}). \tag{5.7}$$

There is an additional solution which increases proportionally to $Y^{\dagger -1}$ in the limit $Y^\dagger \to 0$, since (5.5) is a nonlinear,

$$\psi_3 = \pm\left(\frac{1}{2\alpha Y^\dagger} + \frac{\alpha Y^\dagger}{3} + o(Y^\dagger)\right). \tag{5.8}$$

It can easily be verified, as follows, that the solutions ψ_2 and ψ_3 do not satisfy the zero flux boundary condition in the limit $Y^\dagger \to 0$. The pair correlation function is $\chi = (\chi_o/\psi^2)$, and the temperature field is substituted using (5.2) to obtain the heat flux at the top surface,

$$q = -K\frac{\mathrm{d}T}{\mathrm{d}Y} = -\frac{K_c(6\phi_c g\delta\cos(\theta))^{3/2}}{(\pi p_c)^{3/2}}\frac{Y^{\dagger 1/2}}{\psi}\frac{\mathrm{d}(Y^\dagger\psi^2)}{\mathrm{d}Y^\dagger}. \tag{5.9}$$

It is easy to verify that the zero flux condition is satisfied in the limit $Y^\dagger \to 0$ only for the solution ψ_1 in (5.6), whereas the flux approaches a constant value in the limit $Y^\dagger \to 0$ for ψ_2, and diverges in the limit $Y^\dagger \to 0$ for ψ_3. Therefore, the only solution for (5.5) which satisfies the zero flux boundary condition is $\psi = \psi_1$, in which the constant C is determined from the requirement that the function approaches $\psi = 1 (\chi = \chi_o)$ in the limit $Y^\dagger \to \infty$. Equation (5.5) cannot be solved analytically, but has to be solved numerically in order to determine ψ as a function of $Y^\dagger$. The numerical solution is complicated owing to the stiff nature of the equation, and we use a shooting method in order to determine the value of the constant C required to obtain $\psi = 1$ for $Y^\dagger \to \infty$. Owing to the divergence of the solution (5.6) in the limit $Y^\dagger \to \infty$, and the stiff nature of (5.5), we obtain a solution in the domain $0.0001 \leqslant (\alpha Y^\dagger) \leqslant 10$, with the boundary condition $\Psi = (C/(\alpha Y^\dagger)^{1/2})$ and $(\mathrm{d}\Psi/\mathrm{d}(\alpha Y^\dagger)) = -C/(2(\alpha Y^\dagger)^{3/2})$. The value of the constant C required to satisfy the condition for $(\alpha Y^\dagger) = 10$ turns out to be 0.744, and the solution for the function $\psi = \Psi(\alpha Y^\dagger)$ is shown in figure 9. A polynomial approximation for Ψ in the domain $0 \leqslant (\alpha Y^\dagger) \leqslant 5$, which is correct to within $\pm 0.5\,\%$, is

$$\Psi(\alpha Y^\dagger) = ((\alpha Y^\dagger)^{-1/2})(0.742498 + 0.410196(\alpha Y^\dagger) - 0.0213402(\alpha Y^\dagger)^2 - 0.00272469(\alpha Y^\dagger)^3 + 0.000817992(\alpha Y^\dagger)^4 - 0.0000585208(\alpha Y^\dagger)^5). \tag{5.10}$$

This completes the solution of the volume fraction and temperature profiles at the top boundary layer.

We now return to the comparison of the length scales for the variation of the density and the temperature. The asymptotic solution obtained above predicts that $\psi \propto Y^{\dagger -1/2}$ in the limit $Y^\dagger \to 0$, and therefore the pair distribution function decreases

https://doi.org/10.1017/S002211200700002X Published online by Cambridge University Press

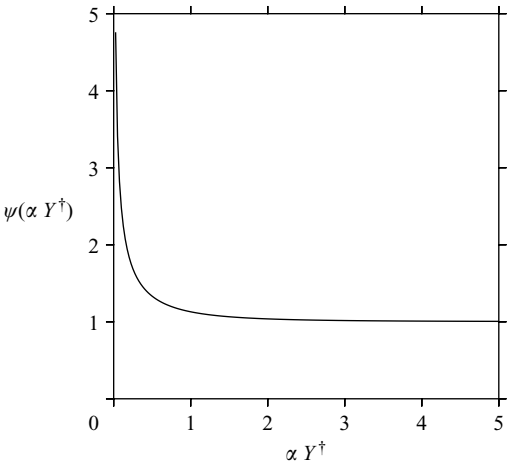


FIGURE 9. The function $\Psi(\alpha Y^{\dagger})$, which is the solution of (5.5), as a function of $\alpha Y^{\dagger}$.

as $\chi = \chi_o Y^{\dagger}$. However, it should be noted that the minimum pair distribution function in the dilute limit is 1, and the pair distribution function cannot decrease below 1. Therefore, the boundary layer solution is valid only for $Y^{\dagger} > \chi_o^{-1}$, where χ_o is large compared to 1 for a dense flow. In the region where the density decreases to zero, the pair correlation function $\chi \sim 1$, and the coordinate $Y^{\dagger} \sim \chi_o^{-1}$. Therefore, the length scale for the decrease of the density is (δ/χ_o). This length scale for the decrease of the density can also be derived in another manner. The temperature approaches a constant value, proportional to $(\phi_c g \delta \cos(\theta)/(p_c - B_c G_c^2)\chi_o)$ in the limit $Y^{\dagger} \to 0$, as indicated by the scaling in (5.2). When the volume fraction is small, the pair correlation approaches 1, and the length scale can be derived from the momentum conservation (5.2). The pressure is proportional to the volume fraction ϕ in the limit $\phi \ll 1$, and therefore the length scale obtained by a balance between the pressure gradient at a location and the weight of material above that location is $(T/g) \sim (\delta/\chi_o)$. Therefore, the length scale over which the density decreases to zero is (δ/χ_o), which is small compared to the length scale for the variation in the temperature, δ, as anticipated earlier.

A uniform approximation can now be obtained for the temperature field which is valid in the bulk and both the boundary layers using asymptotic matching. The solution (4.26), written in terms of the coordinate system with origin at the top of the boundary flowing layer, is

$$T = \frac{6\phi_o g \cos(\theta)}{\pi(p_c - B_c G_c^2)\chi_o} \left(h \left(\frac{1 - c\exp(-\alpha y/\delta)}{1 + c\exp(-\alpha y/\delta)} \right)^2 - y \right). \tag{5.11}$$

The solution (5.2), with $(\chi/\chi_o) = (1/\Psi(Y^{\dagger})^2)$, is

$$T = \frac{6\phi_o g (h - y)\cos(\theta)}{\pi(p_c - B_c G_c^2)\chi_o \Psi(\alpha(h - y)/\delta)^2}. \tag{5.12}$$

When we add the two solutions (5.11) and (5.12), and subtract the common limit, which is the value of (5.11) in the limit $(h - y) \to 0$ or the value of (5.12) in the limit

https://doi.org/10.1017/S002211200700002X Published online by Cambridge University Press

$((h-y)/\delta)\to\infty$, we obtain,

$$T=\frac{6\phi_o g\cos(\theta)}{\pi(p_c-B_cG_c^2)\chi_o}\left(h\left(\left(\frac{1-c\exp(-\alpha y/\delta)}{1+c\exp(-\alpha y/\delta)}\right)^2-1\right)+\frac{(h-y)}{\Psi(\alpha(h-y)/\delta)^2}\right). \quad (5.13)$$

From the above temperature profile, the pair correlation function is determined from (5.2), and the volume fraction is determined from the pair correlation function.

6. Uniform approximation

The above boundary layer solutions indicate a uniform approximation that could be used to describe the flow of thinner but dense layers, where the separation between the conduction length δ and the layer height h is not large. We use the relations for the pressure, viscosity and dissipation coefficient, which are correct to leading order in an expansion in χ^{-1}. Using the approximation (4.14) and (4.17) for the viscometric coefficients and the ratio of production and dissipation, the momentum balance equation in the vertical direction becomes

$$T=\frac{6}{\pi}\frac{\phi g Y\cos(\theta)}{(p_c-B_cG_c^2)\chi} \quad (6.1)$$

where Y is the coordinate from the top of the granular layer, as shown in figure 1. We simplify the temperature equation (6.1) by assuming $\phi=\phi_o$. As noted while determining the boundary layer solution at the top surface in the previous section, this assumption is not valid in a region of thickness (δ/χ_o) at the top surface, where the density decreases from ϕ_o to zero, but is valid in the bulk of the flow and the bottom boundary layer. If this is inserted into the energy conservation equation, with the approximation (4.17) for the difference between the shear production and energy dissipation, we obtain

$$\frac{\mathrm{d}}{\mathrm{d}Y}\left(\frac{K_c}{d^2}\chi^{1/2}Y^{1/2}\frac{\mathrm{d}}{\mathrm{d}Y}\left(\frac{Y}{\chi}\right)\right)=-\frac{R_cD_c\varepsilon^2}{d^4}\frac{Y^{3/2}}{\chi^{1/2}}\left(\frac{1}{\chi}-\frac{1}{\chi_o}\right). \quad (6.2)$$

Using the substitution $\chi=(\chi_oY/hv^2)$, we obtain

$$\frac{\mathrm{d}^2v}{\mathrm{d}Y^2}+\frac{1}{Y}\frac{\mathrm{d}v}{\mathrm{d}Y}+\frac{R_cD_c\varepsilon^2}{2K_c\chi_od^2}\left(v-\frac{hv^3}{Y}\right)=0. \quad (6.3)$$

If we scale the Y coordinate by the total height h, we obtain a nonlinear differential equation for v,

$$\frac{\mathrm{d}^2v}{\mathrm{d}Y^{*2}}+\frac{1}{Y^*}\frac{\mathrm{d}v}{\mathrm{d}Y^*}+Ah^2\left(v-\frac{v^3}{Y^*}\right)=0 \quad (6.4)$$

where $Y^*=(Y/h)$, and the parameter $A=(R_cD_c\varepsilon^2/2K_c\chi_od^2)$. The boundary conditions at the top surface $Y=0$ and at the bottom surface $Y=h$ can be expressed in terms of the variable v,

$$\left.\begin{aligned}\frac{\mathrm{d}v}{\mathrm{d}Y^*}&=0 \text{ at } Y^*=0,\\ \frac{\mathrm{d}v}{\mathrm{d}Y^*}&=\frac{\beta hv}{2} \text{ at } Y^*=1.\end{aligned}\right\} \quad (6.5)$$

The relationship between the approximate equation (6.4) and the asymptotic solution (5.13) can be inferred by recognizing that the parameter $A=(\alpha/\delta)^2$, where

https://doi.org/10.1017/S002211200700002X Published online by Cambridge University Press

$\alpha = (R_c D_c / 2K_c \chi_o)^{1/2}$ was used in (5.13). In the limit $h \gg \delta$, the parameter Ah^2 is large compared to 1, and the solution for (6.4) is $v = \sqrt{Y^*}$. This is identical to the outer solution,

$$\chi = \chi_o, \quad T = \frac{6}{\pi} \frac{\phi_o g Y \cos(\theta)}{(p_c - B_c G_c^2)\chi_o}. \tag{6.6}$$

The boundary layer solutions can also be derived by carrying out an asymptotic expansion of (6.4) about $Y = 0$ and $Y = h$, and using the boundary conditions (6.5).

7. Results

The results of the boundary layer analysis, equation (5.13), and the results of the simplified equation, (6.4), are compared here with the results of the complete momentum and energy equations (3.1) and (3.3). From the results of § 3, boundary layer solutions exist over a larger range of coefficients of restitution for the partially rough particle model, and so we use this model for the present results. It should be noted that boundary layer solutions do not exist for nearly elastic particles in the limit $\varepsilon \to 0$, but exist only when the coefficients of restitution are below a maximum value. For the partially rough particle model and the hard-sphere pair correlation function, this maximum coefficient of restitution e_n is a little less than 0.9. Therefore, we are constrained to use coefficients of restitution less than about 0.9, though the boundary layer analysis has been carried out in the limit $\varepsilon = (1 - e_n)^{1/2} \to 0$.

In the numerical solution of the governing equations (3.1) and (3.3), we express the volume fraction in terms of the pair distribution function using (2.7), and then solve for the pair distribution function and the temperature profiles. The viscometric coefficients were expanded in a series in the small parameter χ_o^{-1}, and the leading-order, first and second corrections were retained for the purposes of the calculation. A Chebyschev collocation technique was used for solving (3.1) and (3.3), as well as the simplified equation (6.4). The number of collocation points is 100 over the interval $y = 0$ to $y = h$ in all the results reported here. It was verified that the values of the maximum temperature did not vary by more than 1 % when the number of collocation points was changed from 100 to 200. For the purposes of graphical representation we define a scaled temperature T^*,

$$T = T^* \frac{6\phi_o g h \cos(\theta)}{\pi (p_\phi - B_\phi G^2)|_{\phi=\phi_o}}. \tag{7.1}$$

This scaled temperature is defined so that $T^* = (1 - (y/h))$ for the outer solution. The scaled strain rate is defined as

$$\dot{\gamma} = \frac{\dot{\gamma}^*}{G} \left(\frac{6\phi_o g h \cos(\theta)}{\pi (p_\phi - B_\phi G^2)|_{\phi=\phi_o}} \right)^{1/2}. \tag{7.2}$$

The scaled strain rate is defined so that $\dot{\gamma}^* = (1 - (y/h))^{1/2}$ for the outer solution.

Figure 10 shows typical profiles for the temperature, volume fraction and pair distribution function for a layer of thickness 40 particle diameters and bulk volume fraction $\phi_o = 0.6$, and $(\beta d) = 1$ in boundary condition (4.9). The numerical solution of the complete momentum and energy conservation equations (3.1) and (3.3), were used for obtaining these results. Figure 10 also shows the ratio of the scaled temperature and the outer solution, $T^* = (1 - (y/h))$. It is observed that the pair distribution function increases in the bottom boundary layer in the region where the temperature

https://doi.org/10.1017/S002211200700002X Published online by Cambridge University Press

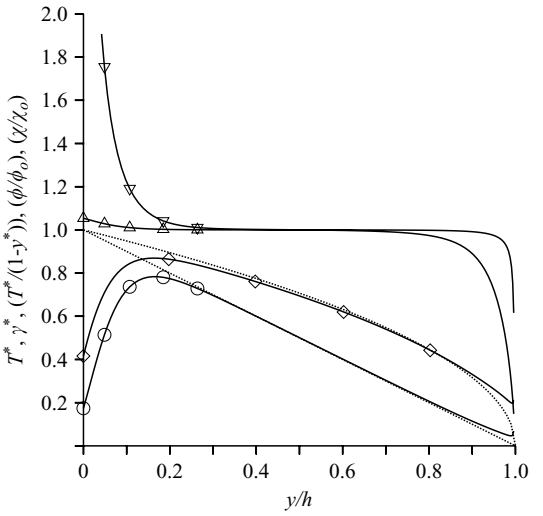


FIGURE 10. The scaled temperature T^* (equation (7.1)) ($\bigcirc$), the ratio of the actual temperature and the outer solution, $T^*/(1-(y/h))$ ($\diamond$), the ratio of the volume fraction and its bulk value, ϕ/ϕ_o ($\triangle$), and the ratio of the pair distribution function and its bulk value, χ/χ_o ($\triangledown$), as a function of (y/h) for a flow with bulk volume fraction $\phi_o = 0.6$, bulk pair distribution function $\chi_o = 21.34$, and angle of inclination $\theta = 19.92°$. The broken lines shows the leading-order solution for the temperature, $T_o^* = (1-(y/h))$, and the strain rate, $\dot{\gamma}_o^* = (1-(y/h))^{1/2}$.

decreases due to the dissipative nature of the boundary, but there is very little change in the volume fraction at this boundary. This is due to the rapid variation of the pair distribution function with volume fraction as the limit of close packing is approached. At the top boundary, it is observed that there is a relatively large variation in the ratio of the temperature and the leading approximation, $(T^*/(1-(y/h)))$, even though the absolute value of T^* is small, because the leading approximation approaches zero at $y = h$. The scaled strain rate $\dot{\gamma}^*$ shows an initial increase at the base, and is then close to the outer solution $(1-(y/h))^{1/2}$ in the bulk. However, there is a substantial difference between the scaled strain rate and the outer solution in the top boundary layer, and the scaled strain rate does not decrease to zero at the top surface. The graph of $(T^*/(1-(y/h)))$ also shows that the thickness of the boundary layers at the top and bottom are of equal magnitude. It is observed that the length scale for the evolution of the temperature and the pair distribution function to their bulk values are comparable, whereas the length scale for the evolution of the volume fraction to its bulk value at the top is much smaller.

One of the assumptions made while deriving the boundary layer solution at the top surface was that the length scale for the decrease of the volume fraction to zero is small compared to the length scale for the decrease of the pair distribution function. The assumption can be quantitatively tested as follows. First, we define two length scales, l_ϕ and l_χ as the distance from the top surface at which $\phi = 0.95\phi_o$ and $\chi = 0.95\chi_o$. Though the factor 0.95 is arbitrary, the length scales provide some indication of the distance over which the volume fraction and the pair distribution function evolve to their bulk values. The ratio of these length scales and the particle diameter are shown in figure 11 as a function of $(\phi_c - \phi_o)$, where $\phi_c = 0.64$ is the volume fraction for close packing, and ϕ_o is the bulk volume fraction. It is observed that l_ϕ decreases for $\phi \to \phi_c$, whereas l_χ increases in this limit. Figure 11 also shows the ratio (l_χ/l_ϕ),

https://doi.org/10.1017/S002211200700002X Published online by Cambridge University Press

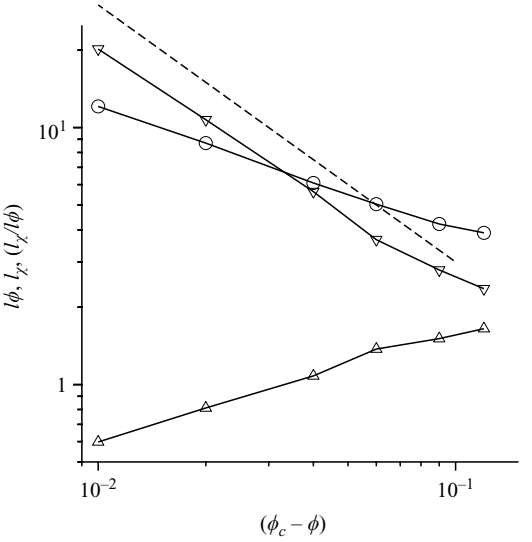


FIGURE 11. The length scales l_ϕ ($\triangle$), l_χ ($\bigcirc$), both scaled by the particle diameter d, and the ratio l_χ/l_ϕ ($\triangledown$) as a function of $(\phi_c - \phi)$, where $\phi_c = 0.64$ is the volume fraction at close packing. The broken line shows a slope of -1.

which increases proportionally to $(\phi_c - \phi_o)^{-1}$. Note that the pair correlation function χ_o, equation (2.7), also increases as $(\phi_c - \phi_o)^{-1}$ in the limit $\phi_c \to \phi_o$. Thus, this verifies the assumption made in the asymptotic analysis that the length scale for the decrease of the volume fraction to zero at the top of the layer is $O(\chi_o^{-1})$ smaller than the boundary layer thickness over which the pair distribution function decreases to zero, and the volume fraction profile can be considered to be a step function over length scales comparable to the boundary layer thickness.

The details of the temperature and density variations near the top boundary layer, which are not clearly visible in figure 10, are shown in figure 12. It should be noted that for the boundary layer at the top, we had used the condition that the flux is zero at $Y = 0$ for choosing the boundary layer solution ψ_1 in equation (5.6). However, this was not equivalent to a zero temperature gradient; it can easily be verified that the temperature gradient is non-zero at the top owing to the first correction proportional to $C^3(\alpha Y^\dagger)^{1/2}$ in (5.6) for ψ_1. The flux decreases to zero because the pair correlation function $\chi = (\chi_o/\psi_1^2)$ decreases to zero, and consequently the thermal conductivity goes to zero. This is a consequence of the assumption that the flow is dense, and so only the leading term in the expression for the conductivity proportional to χ has been retained. As the pair correlation function decreases, there is a transition from a dense to a dilute flow, and then to a ballistic layer.

It is clear from figure 12(b) that there is close agreement between the asymptotic solution (5.13) and the solution of the simplified equation (6.4) in the upper boundary layer, since both have made use of the large-χ approximation. The temperature predicted by the numerical solution depends on the boundary condition we impose at the top. If the zero temperature condition is imposed, the temperature is lower than that from the simplified equation (6.4), whereas if we impose a zero flux condition, the temperature is higher than that of the simplified equation (6.4). The trend observed in the numerical solution with the zero flux condition is consistent with the simulations of Silbert *et al.* (2001), which find an increase in temperature near the top surface.

https://doi.org/10.1017/S002211200700002X Published online by Cambridge University Press

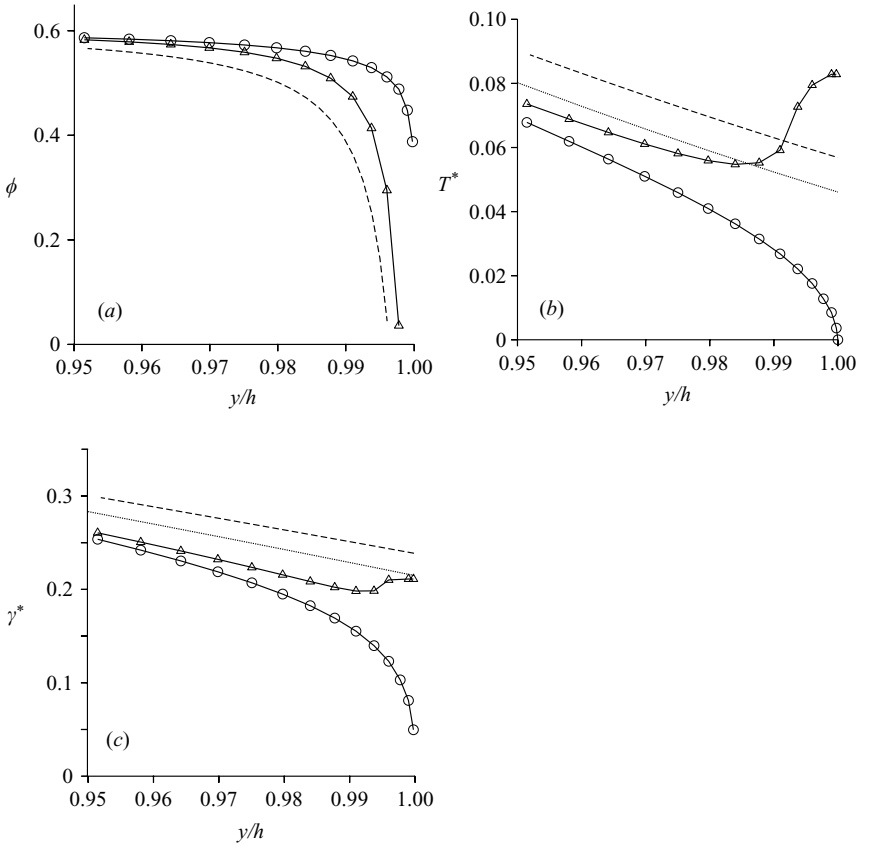


FIGURE 12. (*a*) Volume fraction, (*b*) scaled temperature and (*c*) scaled strain rate in the upper boundary layer region for a flowing granular layer with $h = 40d$, $e_n = 0.8$, $e_t = 1.0$, and volume fraction for the outer solution $\phi_o = 0.6$ for $\beta d = 1.0$ in the boundary condition (4.9). Results for other values of β are indistinguishable from these. The solid lines show the results of the numerical solution of the momentum and energy equations, (3.1) and (3.3), with the zero temperature boundary condition at the top surface (○), and the zero flux condition at the top surface (△). The broken lines show the results of the solution of the approximate equation (6.4), and the dotted lines show the asymptotic solution (5.13). The asymptotic results are not shown in (*a*) for clarity.

Though this has been attributed to a term in the energy flux equation which is proportional to the gradient in the temperature (Brey, Ruiz-Mantero & Moreno 2001; Soto, Mareschal & Risso 1999), we observe this increase even when the term proportional to the temperature gradient is not included. Further work is required to resolve this difference, and to identify the elements in the full equations responsible for this increase which were neglected when the approximate equation (6.4) was derived. Theoretically, there are two issues which need to be examined – the effect of the neglected terms in the expressions for the viscometric coefficients in the region where the pair distribution function is $O(1)$, and the applicability of kinetic theory in the ballistic layer at the top. It can also be seen from figure 12(*a*) that the spacing between grid points is becoming of the same magnitude as the thickness of the region over which the density decreases, even when we have used a hundred Chebyschev collocation points. More sophisticated numerical techniques may also be required to resolve the sharp density variations at the upper boundary.

https://doi.org/10.1017/S002211200700002X Published online by Cambridge University Press

It is clear that there are difficulties with numerical resolution at the upper boundary, and the variation in the temperature predicted by the numerical solution of (3.1) and (3.3), is not captured by the solution of the simplified (6.4) or the boundary layer solution (5.13). However, other aspects of the numerical solution are in agreement with the asymptotic analysis. It is found that the length scale for the decrease in the density is small compared to the boundary layer thickness. Further, in the numerical solutions, the density and temperature profiles in the bulk and the bottom boundary layer are not affected by the small variations due to different boundary conditions at the top. The numerical solutions and those of the approximate equation show some difference only in a region of thickness less than a particle diameter at the top. This indicates that the bulk of the flow and the bottom boundary layer are adequately captured by the simplified equation (6.4).

The variation of the strain rate at the top of the boundary layer is shown in figure 12(c). Once again, it is observed that there is close agreement between the solution of the simplified equation (6.4) and the asymptotic solution (5.13), though the numerical solution of equations (3.1) and (3.3) depends on the boundary conditions imposed at the top. There is a slight increase in the strain rate at the top if a zero temperature gradient condition is imposed, but the strain rate decreases to zero if the zero temperature condition is imposed. The non-zero strain rate at the top could be the reason for the difference in rheology between the bulk and the surface layer that has been reported previously. If the stress is given by the Bagnold law, and there is no deviation from this law at the top surface, then the strain rate is proportional to $(h-y)^{1/2}$, and the velocity profile which satisfies the zero velocity condition at the base is proportional to $(h^{3/2}-(h-y)^{3/2})$. However, if the strain rate approaches a constant value at the top surface $y=h$, then the velocity profile has an additional component which is a linear function of distance from the top surface. This could be the reason for previous observations of a linear velocity profile in the top surface layer, and a Bagnold profile in the bulk.

The effect of the temperature boundary conditions at the bottom boundary is shown in figure 13 for different values of the parameter (βd) in the boundary condition (4.9). It is observed that the temperature increases near the base when (βd) is negative (energising base), while it decreases near the base when (βd) is positive (dissipative base). Figure 13(a) shows that the volume fraction profile is remarkably flat in the bulk of the flow, though there are variations near the base due to the temperature boundary condition. The temperature profiles are shown in figure 13(b). The results of the full numerical solution for $(\beta d)=-1.0$ are not shown, because the gradient at the base becomes very large and convergence could not be obtained with the Chebyschev collocation code used here. For all other values of (βd), there is close agreement between the numerical results (3.1) and (3.3), and the solutions of the simplified equation (6.4). There is also good agreement between the asymptotic results (5.13) and the numerical results, though this agreement becomes poorer when the base is highly dissipative. Interestingly, the temperature from the numerical solution is closer to a linear profile than the asymptotic solution (5.13) and the solution of the simplified equation (6.4) when the base is dissipative. It is observed that the strain rate decreases at the base if the base is dissipative, and increases if the base is energetic. For a very energetic base, the strain rate is large at the base, indicating that the velocity profile may resemble that obtained from a slip boundary condition. In the reminder of the results section, we use the case $(\beta d)=1$, in order to examine the effects of variations in volume fraction, height and coefficients of restitution.

https://doi.org/10.1017/S002211200700002X Published online by Cambridge University Press

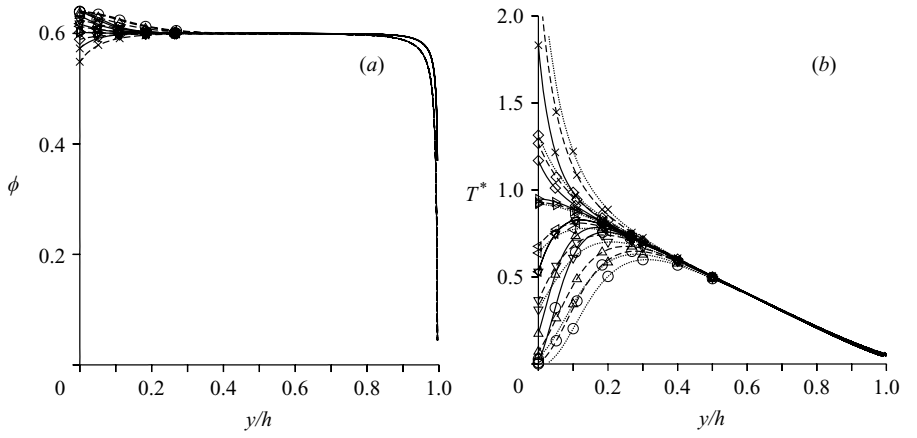


FIGURE 13. (*a*) Volume fraction and (*b*) scaled temperature as a function of height for a flowing granular layer with $h = 40d$, $e_n = 0.8$, $e_t = 1.0$, and volume fraction for the outer solution $\phi_o = 0.6$, corresponding to angle of inclination 19.91°, for different values of the parameter (βd) in the boundary condition (4.9). ○, $\beta d = 3.0$; △, $\beta d = 1.0$; ▽, $\beta d = 0.3$; ◁, $\beta d = 0.1$; ▷, $\beta d = 0.0$; ◇, $\beta d = -0.1$; ×, $\beta d = -0.3$; +, $\beta d = -1.0$. The solid lines show the results of the numerical solution of the momentum and energy equations, (3.1) and (3.3), the broken lines show the results of the solution of the approximate equation (6.4), and the dotted lines show the asymptotic solution (5.13). The asymptotic results are not shown in (*a*) for clarity.

Figure 14 shows the variation in the volume fraction and temperature as the coefficient of restitution is changed for a layer with height equal to 40 particle diameters and with volume fraction for the outer solution $\phi_o = 0.6$. It is observed that the numerical and asymptotic temperature profiles are in good agreement for lower values of the coefficients of restitution, but the agreement becomes poorer, as expected, as the collisions become more elastic. This is because the conduction length $\delta = (d/\varepsilon)$ increases as the coefficient of restitution increases and $\varepsilon = (1 - e_n)^{1/2}$ becomes smaller, and the boundary layer approximation becomes less accurate. Figure 15 shows the variation in the volume fraction and temperature as the volume fraction for the outer solution ϕ_o is changed. The trend in this figure indicates that the agreement between the asymptotic and numerical results is poorer as the volume fraction is increased. Further, the temperature obtained from the asymptotic solution becomes negative at the highest volume fraction $\phi = 0.63$. This is counter-intuitive, because the simplified equation (6.4) was derived using the assumption that the pair correlation function is large, and this assumption should have a greater validity as the volume fraction is increased. The reason for this disagreement is the presence of the factor $\alpha = (\mathscr{R} D_c / 2K_c \chi_o)^{1/2}$ in the asymptotic solution (5.13). It is clear that for an asymptotic solution to be valid, it is necessary that (δ/α) has to be small compared to the total height h in (5.13). As the pair distribution function χ_o increases, α becomes small and the assumption $(\delta/\alpha) \ll h$ becomes invalid when the volume fraction is near close packing. This explains why the agreement between the asymptotic and numerical results becomes poorer as the density increases.

Finally, the variation of the volume fraction and temperature profiles with height h is shown in figure 16. There is good agreement between the solution of the complete equations of motion (3.1) and (3.3), and the solutions of the simplified equation (6.4). The asymptotic solutions (5.13) have a qualitatively similar behaviour to the numerical solution, though the agreement is less good.

https://doi.org/10.1017/S002211200700002X Published online by Cambridge University Press

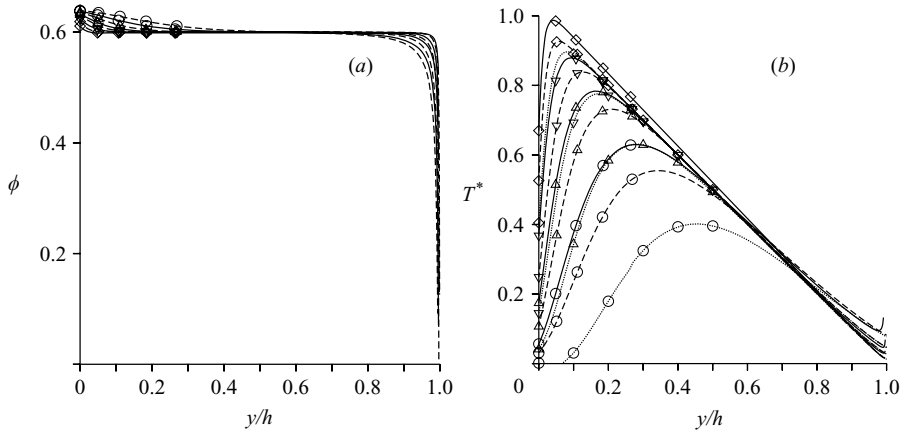


FIGURE 14. (*a*) Volume fraction and (*b*) scaled temperature as a function of height for a flowing granular layer with $h = 40d$, $\beta d = 1.0$ in boundary condition (4.9), the volume fraction for the outer solution is $\phi_o = 0.6$ and for different coefficients of normal and tangential restitution. ○, $e_n = 0.85$, $e_t = 1.0$, $\theta = 18.36°$; △, $e_n = 0.8$, $e_t = 1.0$, $\theta = 19.91°$; ▽, $e_n = 0.7$, $e_t = 1.0$, $\theta = 21.80°$; ◇, $e_n = 0.8$, $e_t = 0.8$, $\theta = 21.58°$. The solid lines show the results of the numerical solution of the momentum and energy equations (3.1) and (3.3), the broken lines show the results of the solution of the approximate equation (6.4), and the dotted lines show the asymptotic solution (5.13). The asymptotic results are not shown in (*a*) for clarity.

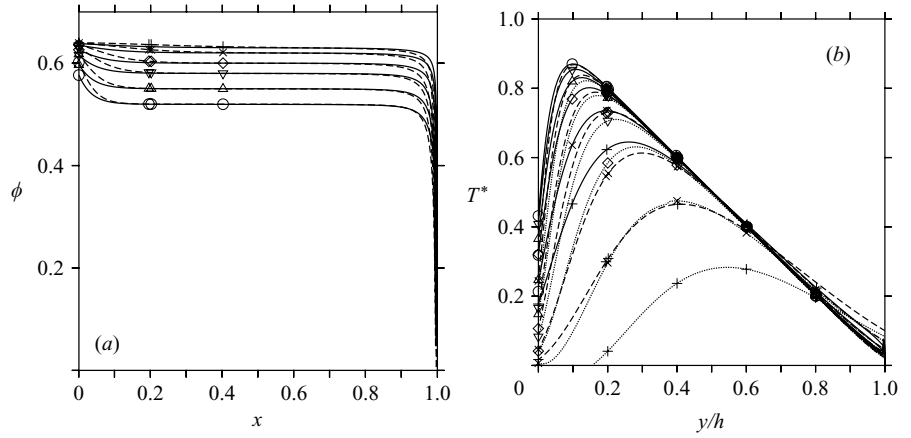


FIGURE 15. (*a*) Volume fraction and (*b*) temperature as a function of height for a flowing granular layer with $h = 40d$, $\beta d = 1.0$ in boundary condition (4.9), $e_n = 0.8$ and $e_t = 1.0$ for different values of the volume fraction for the outer solution is ϕ_o. ○, $\phi_o = 0.52$, $\theta = 20.09°$; △, $\phi_o = 0.55$, $\theta = 20.01°$; ▽, $\phi_o = 0.58$, $\theta = 19.95°$; ◇, $\phi_o = 0.6$, $\theta = 19.91°$; ×, $\phi_o = 0.62$, $\theta = 19.88°$; +, $\phi_o = 0.63$, $\theta = 19.87°$. The solid lines show the results of the numerical solution of the momentum and energy equations, (3.1) and (3.3), the broken lines show the results of the solution of the approximate equation (6.4), and the dotted lines show the asymptotic solution (5.13). The asymptotic results are not shown in (*a*) for clarity.

Since the above comparisons have shown good agreement between the numerical solutions of the complete equations (3.1) and (3.3) and the solution of the approximate equations (6.4), we use (6.4) to further analyse the flow behaviour in the regime where the separation of scales between the flow height and boundary layer thickness is not large. The issue we focus on is a minimum height h_{stop} required for a steady velocity

https://doi.org/10.1017/S002211200700002X Published online by Cambridge University Press

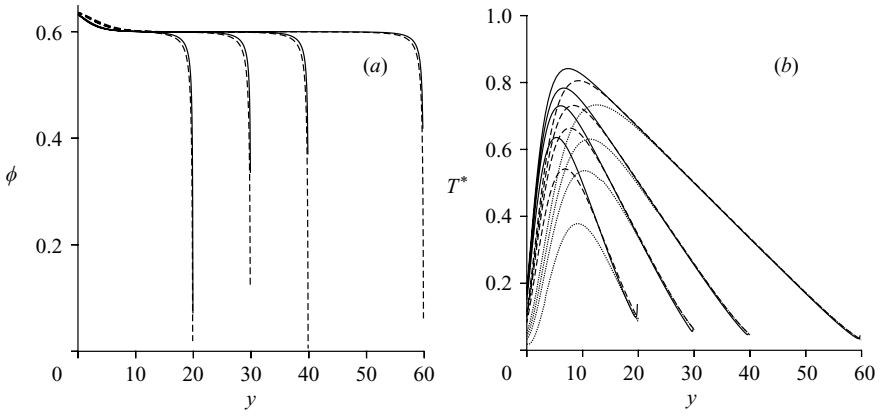


FIGURE 16. (*a*) Volume fraction and (*b*) scaled temperature for a flowing granular layer with $\beta d = 1.0$ in boundary condition (4.9), $e_n = 0.8$, $e_t = 1.0$, and volume fraction for the outer solution $\phi_o = 0.6$ and angle of inclination $\theta = 19.911^\circ$ for different values of h. The solid lines show the results of the numerical solution of the momentum and energy equations, (3.1) and (3.3), the broken lines show the results of the solution of the approximate equation (6.4), and the dotted lines show the asymptotic solution (5.13). The asymptotic results are not shown in (*a*) for clarity.

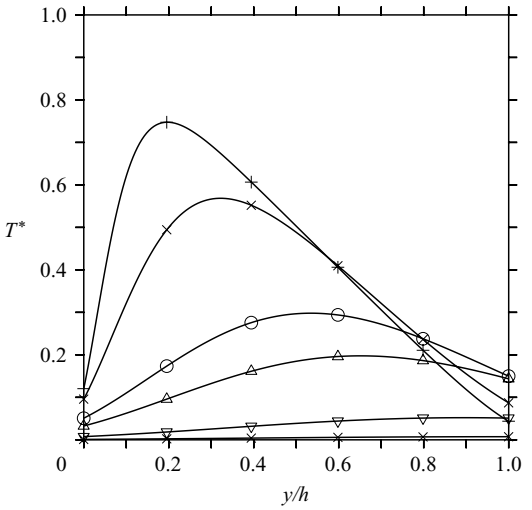


FIGURE 17. The scaled temperature T^* as a function of the scaled height y/h, obtained from a solution of the simplified equation (6.4) with $Ad^2 = 1$, and with $\beta d = 1$ in the boundary condition (4.9), for different values of the total height. +, $h = 40d$; ×, $h = 20d$; ○, $h = 10d$; ▽, $h = 8d$; △, $h = 6d$; ×, $h = 5.6d$. The temperature decreases to zero at $h = 5.55d$.

profile. An energy balance argument can be used to explain the physical reason for the minimum height. An example of the change in the temperature profile as the height is decreased is shown in figure 17. It is observed that the maximum temperature decreases as height decreases, and this temperature reduces to zero throughout the flow at a finite height. The physical reason for this is as follows. The flow is driven by a balance between the source of energy due to the mean shear and the dissipation due to inelastic collisions. There is dissipation of energy due to particle collisions in the flow as well as due to particle collisions with the base in this case, since the

https://doi.org/10.1017/S002211200700002X Published online by Cambridge University Press

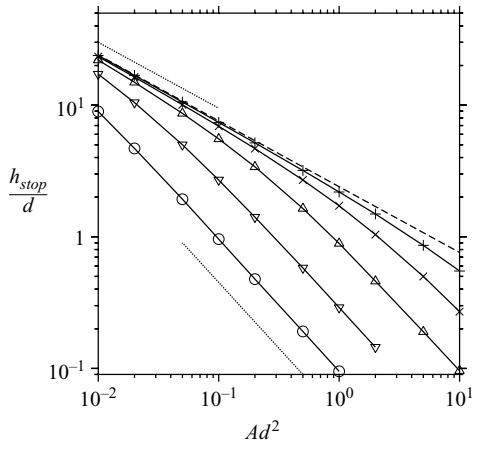


FIGURE 18. The scaled minimum height h_{stop}/d as a function of the parameter Ad^2 in equation (6.4) for different values of the parameter βd in the boundary condition (4.9). ○, $(\beta d) = 0.1$; ▽, $(\beta d) = 0.3$; △, $(\beta d) = 1.0$; ×, $(\beta d) = 3.0$; +, $(\beta d) = 10.0$. The broken line shows h_{stop} for a flow with zero temperature boundary condition at the base. The upper dotted line shows a slope of -0.5, while the lower dotted line shows a slope of -1.0.

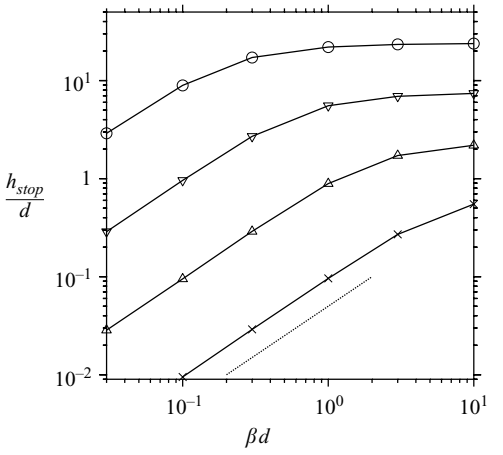


FIGURE 19. The minimum height h_{stop}/d as a function of the parameter βd in equation (4.9) for different values of the parameter Ad^2 in the boundary condition (6.4). ○, $Ad^2 = 0.01$; ▽, $Ad^2 = 0.1$; △, $Ad^2 = 1.0$; ×, $Ad^2 = 10.0$. The dotted line shows a slope of 1.0.

base is dissipative. At constant temperature, the rate of shear production of energy and dissipation in the flow decrease as the layer height decreases, whereas the rate of dissipation in the base does not decrease. Therefore, the temperature has to decrease as the height decreases, and there is a minimum height at which the temperature decreases to zero. Below this height at which the rate of production is not sufficient to compensate for the rate of dissipation in the base, and the flow stops. The height at which the temperature decreases to zero is identified as the minimum height h_{stop}.

The scaled minimum height, (h_{stop}/d), is shown as a function of the parameter Ad^2 in (6.4) for different boundary conditions in figure 18, and as a function of the parameter (βd) in the temperature boundary condition (4.9) in figure 19. It should be noted that values of (h_{stop}/d) below 1 are unrealistic; they are shown so that the

https://doi.org/10.1017/S002211200700002X Published online by Cambridge University Press

scaling of (h_{stop}/d) with (Ad^2) and (βd) can be inferred. The following qualitative features in the limit of low and high dissipation are observed.

(*a*) In the limit of high dissipation, figure 18 shows that $(h_{stop}/d) \propto (Ad^2)^{-1/2}$. The physical reason for this is as follows. When the base is highly dissipative, with $\beta \gg 1$ in the boundary condition (4.9), it is equivalent to having a zero temperature boundary condition at the base. In this case, β ceases to be a parameter in the problem, and the only parameters in equation (6.4) are A and h. By dimensional analysis, it is clear that (Ah^2) has to be a constant when the flow stops, and therefore $h_{stop} \propto A^{-1/2}$. The numerical result for the zero temperature boundary condition is also shown in figure 19, and the following scaling law is obtained from this solution:

$$h_{stop} = 2.4A^{-1/2}. \tag{7.3}$$

(*b*) The minimum height h_{stop} becomes small in the limit of low dissipation, and is identically equal to zero for $\beta = 0$. This is because when there is no dissipation in the base, both the rate of production and dissipation in the granular material decrease proportionally to each other as the height decreases at constant temperature. Figure 19 shows that h_{stop} decreases proportionally to β in the limit $\beta \to 0$. Based on dimensional analysis, the relation for h_{stop} in this limit has to be of the form $h_{stop} = \beta A^{-1}$. The scaling law obtained from figures 18 and 19 in this limit is

$$h_{stop} = 0.95\beta A^{-1}. \tag{7.4}$$

In order to relate the minimum height h_{stop} to the angle of inclination, it is necessary to relate the parameter (Ad^2) to the angle of inclination. Since $(Ad^2) = (R_c D_c \varepsilon^2 / 2K_c \chi_o)$, the dependence of (Ad^2) on the angle of inclination is due to the dependence of the pair distribution function χ_o on the angle of inclination. Note that the limit $\chi_o \gg 1$ corresponds to the limit $(Ad^2) \ll 1$. This relation between the angle of inclination and χ_o was analysed earlier by the author (Kumaran 2006*a*), and a series expansion was derived for $\tan(\theta)$ as a function of $(1/\chi_o)$, where θ is the angle of inclination. The relation between $\tan(\theta)$ and χ_o was of the form

$$\tan(\theta) - \tan(\theta_c) = C_1(\phi_o \chi_o)^{-1} + C_2(\phi_o \chi_o)^{-2} \tag{7.5}$$

where θ_c is the minimum angle at which flow is initiated, and C_1 and C_2 are parameters which depend on the microscopic model used for particle interactions. These parameters are

$$\tan(\theta_c) = \frac{1.02693\varepsilon_r}{\left(0.874417 + \varepsilon_r^2 - 0.437208\varepsilon^2\right)}, \tag{7.6a}$$

$$C_1 = -\frac{0.254845\varepsilon_r\left(0.376137 + 0.252379\varepsilon^2 - \varepsilon_r^2\right)}{\left(0.874417 + \varepsilon_r^2 - 0.437208\varepsilon^2\right)^2}, \tag{7.6b}$$

$$C_2 = \frac{0.121859\varepsilon_r\left(\varepsilon_r^4 + 0.298183\varepsilon_r^2 + 0.307759 - 0.4743089\varepsilon_r^2\varepsilon^2 + 0.033950\varepsilon^4 - 0.020421\varepsilon^2\right)}{\left(0.874417 + \varepsilon_r^2 - 0.437208\varepsilon^2\right)^3}, \tag{7.6c}$$

for rough spheres, where $\varepsilon = (1 - e_n)^{1/2}$, $\varepsilon_r = \varepsilon\sqrt{1 + a_t}$, and

$$\tan(\theta_c) = \frac{0.530463\varepsilon_{pr}}{\left(0.50768 + \varepsilon_{pr}^2 - 0.25384\varepsilon^2\right)}, \tag{7.7a}$$

https://doi.org/10.1017/S002211200700002X Published online by Cambridge University Press

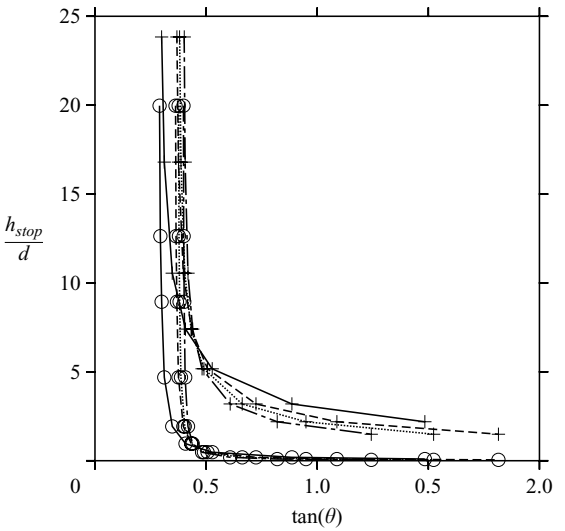


FIGURE 20. The minimum height h_{stop} as a function of $\tan(\theta)$, where θ is the angle of inclination, for different values of the parameter β in the boundary condition (4.9). Results are shown for ○, $\beta = 0.1$, and +, $\beta d = 10.0$; the results for the other values $\beta d = 0.3$; $\beta d = 1.0$ and $\beta d = 3.0$ are in between these two curves. The constitutive relations for the partially rough particle model were used, with coefficients of restitution $e_n = 0.85$ and $e_t = 1.0$ (solid line), $e_n = 0.8$ and $e_t = 1.0$ (broken line), $e_n = 0.7$ and $e_t = 1.0$ (dot-dashed line), and $e_n = 0.8$ and $e_t = 0.8$ (dotted line).

$$C_1 = \frac{0.223654\varepsilon_{pr}\left(\varepsilon_{pr}^2 - 0.087067\varepsilon^2 - 0.126896\right)}{\left(0.50768 + \varepsilon_{pr}^2 - 0.25384\varepsilon^2\right)^2}, \tag{7.7b}$$

$$C_2 = \frac{0.11272\varepsilon_{pr}\left(\varepsilon_{pr}^4 - 0.022895\varepsilon_{pr}^2 - 0.197195\varepsilon_{pr}^2\varepsilon^2 - 0.013628\varepsilon^2 + 0.00889\varepsilon^4 + 0.067511\right)}{\left(0.50768 + \varepsilon_{pr}^2 - 0.25384\varepsilon^2\right)^3}, \tag{7.7c}$$

for partially rough spheres, where $\varepsilon = (1 - e_n)^{1/2}$ and $\varepsilon_r = \varepsilon\sqrt{1 + a_t/4}$. An analytical relation between (Ad^2) and the angle of inclination θ can be obtained if we retain only the term proportional to C_1 in (7.6) and (7.7),

$$(Ad^2) = \frac{R_c D_c \varepsilon^2 (\tan(\theta) - \tan(\theta_c))\phi_o}{2K_c C_1}. \tag{7.8}$$

This relation provides a first approximation for the parameter (Ad^2) in terms of the angle of inclination, and it is useful to first examine the variation of h_{stop} with the angle of inclination using this approximation. For a highly dissipative base, figure 18 shows that $(h_{stop}/d) \propto (Ad^2)^{-1/2}$. Inserting this into (7.8), we obtain the scaling

$$\frac{h_{stop}}{d} \propto (\tan(\theta) - \tan(\theta_c))^{-1/2} \tag{7.9}$$

for $(\beta d) \gg 1$. For a base with less dissipation, figure 18 shows that $(h_{stop}/d) \propto (Ad^2)^{-1}$. Inserting this into (7.8), we obtain the scaling

$$\frac{h_{stop}}{d} \propto (\tan(\theta) - \tan(\theta_c))^{-1} \tag{7.10}$$

https://doi.org/10.1017/S002211200700002X Published online by Cambridge University Press

for $(\beta d) \ll 1$. Quantitative results for (h_{stop}/d) as a function of $\tan(\theta)$ for the partially rough particle model, using (7.7) for the relation between $\tan(\theta)$ and χ_o, are shown in figure 20. It is observed that in all cases, h_{stop} increases as the angle of inclination is decreased, and diverges at a finite angle $\theta = \theta_c$. Further, figure 20 shows that the angle θ_c does not vary much when the coefficients of restitution are 0.8 or below, and the minimum height h_{stop} also shows little variation with the coefficient of restitution for this model.

8. Conclusions

At the outset, it is important to clarify the basic assumptions made to obtain the present results. The basic equations are the momentum and energy conservation equations, in which the stress and heat flux are given by constitutive relations derived from kinetic theory (Kumaran 2006*a*). The boundary conditions are of a form first proposed by Jenkins & Richman (1985), which is widely used in the literature. The constitutive relations were derived using the Enskog approximation, which states that the pair distribution function is the product of the single-particle distribution functions. The Enskog approximation incorporates the reduction in the free volume as a gas becomes dense, and includes the pre-collisional correlations in particle positions through the pair distribution function, but does not include the pre-collisional correlations in the velocities of particles. An earlier study (Kumaran 2006*c*) showed that these correlations do not change the form of the constitutive relations, but could change the numerical values. This is in contrast to elastic fluids, where studies by Ernst *et al.* (1978) have shown that correlations cause a logarithmic dependence of the stress on the strain rate in two dimensions, and a 3/2 power dependence in three dimensions, whereas the Chapman–Enskog procedure predicts that the viscous term is proportional to the strain rate and the Burnett term is proportional to the square of the strain rate. In addition, the pair correlation function was assumed to be of the form reported in the literature for a dense gas of hard spheres at equilibrium. It is known that shear could change the form of the pair correlation function, which could result in changes in the numerical values of the results reported here. However, the qualitative features of the present results, which depend only on the forms of the constitutive relations used and not the values of the viscometric coefficients, are likely to be robust.

In the present analysis, the issue that is not satisfactorily resolved is the boundary layer at the top surface. The modelling of this boundary layer is complicated by the fact that there is a transition from a dense flow to a ballistic regime, and the dynamics in the ballistic regime cannot be modelled using constitutive relations obtained for dense flows. In the boundary layer analysis, two length scales at the top surface were postulated: the conduction length δ over which there is a deviation in the temperature from its linear profile, and a smaller length (δ/χ_o) over which the density decreases at the top surface. The latter was obtained based on the estimate that the pair distribution function is $O(1)$ for the dilute flow at the top, together with the linear decrease in temperature with height in the bulk of the flow. Note that (δ/χ_o) is also the thickness of the ballistic layer, or the maximum height that a particle at the top will travel ballistically if it has a temperature $T \sim (g\delta/\chi_o)$. So this simple scaling analysis indicates that the thickness of the ballistic layer is small compared to the conduction length. The analysis in § 4 only addressed variations over the length scale δ in order to obtain the temperature profile, and assumed that the volume fraction is a step function when viewed on this scale. Simulations of the complete equations

https://doi.org/10.1017/S002211200700002X Published online by Cambridge University Press

do reveal structure in the temperature profile at a length scale small compared to δ, which is not captured by the asymptotic analysis or the simplified equations, though the magnitude of the temperature is correctly predicted by the scaling analysis. A similar behaviour is observed in simulations (Silbert *et al.* 2001), though it is not clear if the increase in temperature at the top surface occurs in the dense layer or in the ballistic layer. The comparison between the asymptotic and numerical results clearly reveals that some elements present in the complete momentum and energy equations are not present in the asymptotic solutions, and a more sophisticated asymptotic analysis is required to capture these. In addition, the asymptotic analysis should be able to match the flow in the dense layer with that in the ballistic layer, in order to satisfactorily resolve the boundary layer flow in the top surface. However, the present analysis has revealed that apart from the layer of thickness (δ/χ_o) at the top, the temperature and density profiles in the reminder of the flow are adequately captured by the asymptotic analysis and the simplified equation (6.4). This indicates that the flow within the bulk is not sensitive to the boundary conditions applied at the top.

At the bottom boundary, the analysis predicts that the temperature and strain rate decrease if the boundary is dissipative, and increase if the boundary is energetic. In addition, there is a small increase in the density, as shown in figure 10, if the boundary is dissipative, and a slight decrease if the boundary is energetic. The variation of the temperature and the strain rate are in agreement with the results of simulations (Silbert *et al.* 2001; Delannay *et al.* 2007) for a dissipative base, but the simulations report that the volume fraction is either a constant or is decreasing slightly as the bottom base is approached. One reason for this discrepancy could be that the governing equations assumed here are too simplistic, and it is necessary to incorporate the higher moments of the velocity distribution function in order to capture the variations of the angular velocity and the translational and rotational temperatures. Another reason could be the layering of the particles at the base which is observed in the simulations, due to the presence of the flat base. This could induce a layered structure near the base which is different from the random structure that is assumed in this analysis.

It is also observed that the angle of inclination varies only by about 0.2° when the volume fraction changes from 0.52 to 0.62 for $e_n = 0.8$ and $e_t = 1.0$ in figure 15. This is considerably smaller than the range between 21° and 25° observed in simulations (Silbert *et al.* 2001). However, it should be emphasized that the present results were obtained with the partially rough particle model of Kumaran (2006*a*), which is not identical to that in the simulations. Therefore, it is not possible to get agreement for the stresses and the angle of inclination quantitatively, just as the stress obtained using the viscometric parameters for one fluid cannot be used to quantitatively predict that in another fluid with a different set of parameters. However, if the rheological models for the two fluids are the same, then the functional forms of the dynamical variables for the two fluids will be the same.

In § 2, the density profile in the bulk of the flow was examined using an asymptotic analysis in the ratio of the conduction length and the thickness of the flowing layer, (δ/h). It was shown that the volume fraction in the bulk is a constant in the leading approximation, and the leading correction to this constant volume fraction is $O(\delta/h)^2$. This correction was evaluated using the rough and partially rough particle models of Kumaran (2006*a*), and was found to be numerically small for a range of parameter values. This provided a satisfactory explanation for the remarkable lack of variation of volume fraction with height observed previously in simulations.

https://doi.org/10.1017/S002211200700002X Published online by Cambridge University Press

The boundary layer at the bottom surface was analysed in § 3, using an inner coordinate which is the distance from the bottom surface scaled by the conduction length. The momentum and energy conservation equations were reduced to a second-order equation for the volume fraction. In the limit where the inner coordinate becomes large, this equation reduces to a diffusion equation. However, it was found that the diffusion coefficient is negative in the limit $e_n \to 1$ and $e_t \to 1$, indicating that the boundary layer solutions cannot be matched to the bulk solution. The diffusion coefficients becomes positive only when the coefficients of restitution decrease below a maximum value. An analytical solution for the boundary layer profiles was obtained for dense flows using the inverse of the pair distribution function as a small parameter. These were found to be in good agreement with numerical solutions of the complete equations. The results obtained in this section also explain a salient feature observed in simulations: that the boundary conditions at the bottom do not affect the density and temperature profiles in the bulk of the flow.

We were able to derive an exact result which establishes a relationship between the existence of boundary layers and the dependence of the volume fraction in the outer region on the angle of inclination. This result states that a boundary layer solution exists if and only if the viscometric parameters are such that the volume fraction decreases as the angle of inclination increases. This implies that a stable flow will not be achieved when the viscometric coefficients are such that the volume fraction increases when the coefficient of restitution increases.

The results of § 3 indicate that the boundary layer solutions exist only when the coefficients of restitution decrease below a maximum value; this value is about 0.75 for rough particles and close to 0.9 for partially rough particles. This is in qualitative agreement with the simulation results of Silbert *et al.* (2001), where it is found that a steady solution is possible only when the coefficient of restitution decreases below about 0.92 for the models used there. It is necessary to be careful when making quantitative comparisons, because friction was included in the model of Silbert *et al.* (2001), but was not included while deriving the constitutive relations used here. But the qualitative features obtained from the boundary layer analysis are certainly observed in the simulations.

The momentum and energy equations were reduced to a second-order nonlinear equation in the dense limit in § 5, using the inverse of the pair distribution function as a small parameter. The solutions of this equation were found to be in quantitative agreement with the solutions of the complete governing equations for the parameter values studied here. This equation was then used to analyse the flows in thin layers. It was found that the nature of the flow for thin layers depends on the nature of the boundary conditions at the bottom surface. If the bottom boundary is dissipative, there is a minimum height at which the temperature reduces to zero, and a steady flow is not possible below this minimum height. This is because at constant temperature, the rates of shear production and dissipation due to particle–particle collisions decrease as the height decreases, but the rate of dissipation due to particle–wall collisions does not decrease. The energy balance can be preserved only if the temperature decreases, and there is a minimum height at which the temperature decreases to zero and the flow stops. Below the minimum height, the rate of production due to shear is not sufficient to compensate for the rate of dissipation. The minimum height h_{stop} was obtained as a function of the angle of inclination, and was also found to be in qualitative agreement with simulation results. The h_{stop} versus $\tan(\theta)$ curves are also found to be relatively insensitive to the coefficients of restitution, so long as the coefficients are less than about 0.85.

https://doi.org/10.1017/S002211200700002X Published online by Cambridge University Press

The present analysis is able to qualitatively reproduce most aspects of the flow down an inclined plane. Some of the results, such as the domains for the existence of boundary layer solutions and the h_{stop} versus angle of inclination curves, are also in reasonable quantitative agreement. However, there are quantitative differences. An important difference is that the temperature profiles in simulations are not as linear as those reported here for the same volume fractions, and the thicknesses of the boundary layers in the simulations appear to be larger. A possible reason for this is that the Torquato expression for the pair correlation function under-estimates the pair correlation function for the sheared state. Note that in the asymptotic solution (5.13), the boundary layer thickness is actually (δ/α), where $\alpha = (R_c D_c/2K_c\chi_o)^{1/2}$. Therefore, if the pair correlation function in the analysis is lower than that in the physical system, the boundary layer thickness in the analysis is also lower. Another reason for quantitative differences is that the pair correlation function used here is spherically symmetric, whereas it is likely to be asymmetric in a shear flow. Further work needs to be done to obtain the pair correlation functions in shear flows, and to incorporate the orientation dependence of the pair correlation function, in order to obtain quantitative predictions.

Finally, the present analysis also suggests the minimal model required for describing the dense flows down an inclined plane. The minimal model consists of the momentum and energy balance equations, and it is necessary to include the dissipation of energy due to inelastic collisions in the energy balance equations. It is necessary incorporate the pressure, viscous stress and the Burnett coefficients in the constitutive relations, in order to obtain physically realistic behaviour. In the dense limit, it is sufficient to retain just the term proportional to the pair distribution function in the viscometric coefficient and the dissipation coefficient. All of these coefficients can be determined using kinetic theory, as was done in Kumaran (2006*a*), or by carrying out simulations using some microscopic model for particle interactions. The one parameter which is more difficult to determine in simulations is the parameter R_c. This is related to first correction to the difference between the shear rate of production and the rate of dissipation due to inelastic collisions in an expansion in the inverse of the pair distribution function. This correction is essential for solving the model equations, since the sign of this parameter determines whether a boundary layer solution is possible. But this parameter is likely to be more difficult to evaluate from simulations, since it involves calculating a small difference between the rates of production and dissipation, both of which are nearly equal to each other. A possible way to evaluate this is to use the temperature variations in the boundary layer to obtain the constant $\alpha = (R_c D_c/2K_c\chi_o)^{1/2}$, and to obtain R_c from the numerically evaluated α.

This research was supported by the Swarnajayanthi Fellowship, Department of Science and Technology, Government of India.

REFERENCES

Anderson, J. D. 2005 Ludwig Prandtl's boundary layer. *Physics Today* **58**, 42–48.

Baran, O., Ertas, D., Halsey, T. C., Grest, G. S. & Lechman, J. B. 2006 Velocity correlations in dense gravity-driven granular chute flows. *Phys. Rev.* E **74**, 051302–051311.

Bocquet, L., Errami, J. & Lubensky, T. C. 2002 Hydrodynamic model for a dynamical jammed-to-flowing transition in gravity driven granular media. *Phys. Rev. Lett.* **89**, 184301–184304.

Bonamy, D., Daviaud, F., Laurent, L., Bonetti, M. & Bouchaud, J. P. 2002 Multiscale clustering in granular surface flows. *Phys. Rev. Lett.* **89**, 034301–034304.

https://doi.org/10.1017/S002211200700002X Published online by Cambridge University Press

Brey, J. J., Ruiz-Montero, M. J. & Moreno, F. 2001 Hydrodynamics of an open vibrated granular system. *Phys. Rev.* E **63**, 061305–061314.

Chapman, S. & Cowling, T. G. 1970 *The Mathematical Theory of Non-Uniform Gases*. Cambridge University Press.

Delannay, R., Louge, M., Richard, P., Taberlet, N. & Valance, A. 2007 Towards a theoretical picture of dense granular flows down inclines. *Nature Materials* **6**, 99–108.

Ernst, M. H., Cichocki, B., Dorfman, J. R., Sharma, J. & van Beijeren, H. 1978 Kinetic theory of nonlinear viscous flow in two and three dimensions. *J. Statist. Phys.* **18**, 237–270.

Ertas, D. & Halsey, T. C. 2002 *Europhys. Lett.* **60**, 931–934.

GDR MiDi 2004 On dense granular flows. *Eur. Phys. J.* E **14**, 341–365.

Jenkins, J. T. 2006 Dense shearing flows of inelastic disks. *Phys. Fluids* **18**, 103307–103315.

Jenkins, J. T. & Askari, E. 1999 Hydraulic theory for a debris flow supported on a collisional shear layer. *Chaos* **9**, 654–658.

Jenkins, J. T. & Richman, M. W. 1985 Grad's 13-moment system for a dense gas of inelastic spheres. *Arch. Rat. Mech. Anal.* **87**, 355–377.

Jenkins, J. T. & Savage, S. B. 1983 A theory for the rapid flow of identical, smooth, nearly elastic particles. *J. Fluid Mech.* **130**, 186–202.

Jop, P., Forterre, Y. & Pouliquen, O. 2006 A constitutive law for dense granular flows. *Nature* **441**, 727–730.

Kumaran, V. 1998 Temperature of a granular material fluidised by external vibrations. *Phys. Rev.* E **57**, 5660–5664.

Kumaran, V. 2004 Constitutive relations and linear stability of a sheared granular flow. *J. Fluid Mech.* **506**, 1–43.

Kumaran V. 2006a The constitutive relations for the granular flow of rough particles, and its application to the flow down an inclined plane. *J. Fluid Mech.* **561**, 1–42.

Kumaran, V. 2006b Kinetic theory for the density plateau in the granular flow down an inclined plane. *Europhys. Lett.* **73**, 1–7.

Kumaran, V. 2006c Velocity autocorrelations and the viscosity renormalisation in sheared granular flows. *Phys. Rev. Lett.* **96**, 258002–258005.

Lois, G., Carlson, J. & Lemaitre, A. 2005 Numerical tests of constitutive laws for dense granular flows. *Phys. Rev.* E **72**, 051303.

Lois, G., Carlson, J. & Lemaitre, A. 2006 Emergence of multi-contact interactions in contact dynamics simulations. *Eur. Phys. Lett.* **76**, 318–324.

Louge, M.-Y. 2003 Model for dense granular flows down bumpy surfaces *Phys. Rev.* E **67**, 061303–061313.

Louge, M.-Y. & Keast, S. C. 2001 On dense granular flows down flat frictional inclines. *Phys. Fluids* **13**, 1213–1233.

Lun, C. K. K., Savage, S. B., Jeffrey, D. J. & Chepurniy, N. 1984 Kinetic theories for granular flow: inelastic particles in Couette flow and slightly inelastic particles in a general flow field. *J. Fluid Mech.* **140**, 223–256.

Mitarai, N. & Nakanishi, H. 2005 Bagnold scaling, density plateau, and kinetic theory analysis of dense granular flow. *Phys. Rev. Lett.* **94**, 128001.

Pouliquen, O. 1999 Scaling laws in granular flows down rough inclined planes. *Phys. Fluids* **11**, 542–548.

Pouliquen, O. 2004 Velocity correlations in dense granular flows. *Phys. Rev. Lett.* **93**, 248001–248004.

Pouliquen, O. & Chevoir F. 2002 Dense flows of dry granular material. *C. R. Phys.* **3**, 163–175.

Reddy, K. A. & Kumaran, V. 2007 The applicability of constitutive relations from kinetic theory for dense granular flows. *Phys. Rev.* E **76**, 061305–061313.

Savage, S. B. & Jeffrey, D. J. 1981 The stress tensor in a granular flow at high shear rates. *J. Fluid Mech.* **110**, 255–272.

Sela, N. & Goldhirsch I. 1998 Hydrodynamic equations for rapid flows of smooth inelastic spheres, to Burnett order. *J. Fluid Mech.* **361**, 41–74.

Sela, N., Goldhirsch, I. & Noskowicz, S. H. 1996 Kinetic theoretical study of a simply sheared two dimensional granular gas to Burnett order. *Phys. Fluids* **8**, 2337.

Silbert, L. E., Ertas, D., Grest, G. S., Halsey, T. C., Levine. D. & Plimpton. S. J. 2001 Granular flow down an inclined plane: Bagnold scaling and rheology. *Phys. Rev.* E **64**, 51302.

https://doi.org/10.1017/S002211200700002X Published online by Cambridge University Press

Silbert, L. E., Grest, G. S., Plimpton S. J. & Levine, D. 2002 Boundary effects and self-organization in dense granular flows. *Phys. Fluids* **14**, 2637–2646.

Silbert, L. E., Landry, J. W. & Grest, G. S. 2003 Boundary effects and self-organization in dense granular flows. *Phys. Fluids* **15**, 1–10.

Silbert, L. E., Grest, G. S., Brewster, R. E. & Levine, A. J. 2007 Rheology and contact lifetimes in dense granular flows. *Phys. Rev. Lett*. **99**, 068002.

Soto, R., Mareschal, M. & Risso, D. 1999 Departure from Fourier's law for fluidized granular media. *Phys. Rev. Lett*. **83**, 5003–5006.

Torquato, S. 1995 Nearest neighbour statistics for packings of hard disks and spheres. *Phys. Rev.* E **51**, 3170–3182.

https://doi.org/10.1017/S002211200700002X Published online by Cambridge University Press